PNAS
www.pnas.org

Supplementary Information for

Abundant phosphorus expected for possible life in Enceladus's ocean.

Jihua Hao*; Christopher R. Glein*; Fang Huang; Nathan Yee; David C. Catling; Frank Postberg; Jon K. Hillier; Robert M. Hazen.

*Jihua Hao; Christopher R. Glein.

Email: hao@ustc.edu.cn; christopher.glein@swri.org

This PDF file includes:

S1. Additional model description

The Cosmic Dust Analyzer (CDA) aboard the Cassini spacecraft detected Na, Cl, and (bi)carbonate as the major salt species of icy plume particles from Enceladus (1). Levels of chlorine are suggested to be between 0.2 mole/kg H_2O or molal (at high carbonate) and 0.05 molal (at low carbonate) (1), which were adopted in our model (**Table S2**). It is notable that this level of Cl is generally higher than the maximum level that would be provided by complete dissolution of Enceladus core material in ocean water (**Table S6**); however, additional Cl could have been accreted in volatile/icy forms rather than solely with rock (2, 3). Na^+ is found to be the dominant cation in salty particles and thus was set to be the charge balance species in our geochemical model. On average, K was suggested to be roughly 100-200 times less abundant than Na in plume particles (1). Here, we set the total concentration of K as 100 times less than that of Na.

Total carbonates ions (HCO_3^- + CO_3^{2-}) are suggested to be 0.01-0.1 molal in Enceladus ocean water (1), which were adopted in this model as low and high C cases, respectively. Note that this parameter is different from dissolved inorganic carbon ($CO_{2,aq}$ + HCO_3^- + CO_3^{2-}) and carbonate alkalinity (HCO_3^- + 2×CO_3^{2-}), which are typically reported in geochemical field studies. However, total carbonates is the parameter that was derived from CDA data. In addition, to assess the effect of total carbonate level on P level, we conducted sensitivity tests by varying total carbonate level from 0.001 to 0.5 molal. In those sensitivity tests, total Cl concentration was set to be 2 times that of total carbonate to maintain consistency with the results of Postberg et al. (2009) (1). Based on data from the Ion Neutral Mass Spectrometer (INMS) aboard the Cassini spacecraft, it was suggested that the $H_{2,aq}/CO_{2,aq}$ ratio in Enceladus's ocean is 0.5-4.7 (4). In our model, we varied log $fO_{2,g}$ (oxygen fugacity) to reach the target $H_{2,aq}/CO_{2,aq}$ ratio (0.5 for low H_2 case; 4.7 for high H_2 case) in the simulated Enceladus ocean water.

Nitrogen in Enceladus ocean water is reported to be predominantly reduced valence (N(-III)) with a N/CO_2 ratio of ~1.5 in the plume gas (4). Here, we define the level of N in terms of total dissolved ammonia (NH_3 + NH_4^+) instead of NH_3 only as 1.5 times that of $CO_{2,aq}$, because interconversion between ammonia species is expected to be much faster than interconversion between CO_2 and carbonates over the degassing timescale (4). In addition, we also varied N (total N/CO_2 ratio from 0.15 to 15) to evaluate the effect of N abundance on the P concentration.

There is a lack of observational data on the abundances of divalent cations (Ca, Mg, and Fe) in the Enceladus ocean (1). However, levels of these cations can affect P concentration because they are major components of common P-minerals whose solubilities can be shifted by the common ion effect. Various lines of evidence suggest the occurrence of water-rock interactions in Enceladus's seafloor (1, 4, 5), which have altered primary silicate minerals into secondary silicate/carbonate/hydroxide minerals as observed in chondrites (6, 7). In addition, molecular $H_{2,g}$, likely generated by water-rock reactions, was detected to be a major species of the plume gas (4), suggesting an overall reducing Enceladus ocean. Under this condition, Fe exists predominantly in reduced form, i.e. Fe(II). In this study, we assumed that activities/concentrations of the key divalent cations are controlled by dissolution of the least soluble common secondary minerals (e.g. carbonates and phyllosilicate minerals (8)).

The fluorine concentration in Enceladus's ocean is currently unknown, but may be limited by the abundance of F in Enceladus's rocky core (**Table S6**). However, there are uncertainties in the solar abundances of halogens (9), and halogens could have been delivered to ice-rock bodies mostly as part of the icy component during accretion (2, 3). Despite these uncertainties, the accreted F/Cl ratio may stay relatively constant because of the similar chemical properties of F and Cl. Therefore, in a first approach, we estimated the F^- concentration in Enceladus's ocean water by scaling the F/Cl ratio in CI chondrite material by the appropriate Cl^- concentration for Enceladus's ocean (see above). The resulting estimate is higher than the level that is predicted by dissolving all fluorine from rocky material into the ocean (**Table S6**); therefore, it represents an upper limit. A second limiting factor for fluorine concentration is precipitation of fluoride minerals, i.e., fluorite (CaF_2) in this study. Fluorite is a common F-host mineral during hydrothermal alteration (10). Thus, fluorine concentration in our model is set to be the lower value between the solubility of fluoride minerals and the estimated level of fluorine based on conservative leaching of F and Cl.

The concentration of silica in Enceladus ocean water has been proposed to correspond to the solubility of quartz in seafloor sediments (8). These authors found that geochemical models based on equilibrium with quartz are consistent with the inferred pH of the ocean, while models

with amorphous silica gave pH values that are too low. Under weathering conditions, silica is primarily released by dissolution reactions of solid silica (e.g., quartz) and silicate minerals (e.g., feldspar, olivine, and pyroxene). In the absence of biological silica precipitation, the efflux of silica from seawater is dominated by diagenetic reactions involving carbonate and clay minerals (11–13). In natural waters on Earth, the level of dissolved silica can go up to the solubility of amorphous silica, above which amorphous silica will quickly precipitate. However, in marine sediments, silica tends to transform into more stable forms, for example, opal and later quartz depending on the duration and temperature of diagenesis (12–14). As a consequence, silica concentration would decrease in pore spaces of marine sediments due to nucleation of secondary silica such as opal and reach levels close to the solubility of cristobalite during early to middle diagenesis (11). It has also been proposed that in the presence of water, amorphous silica would irreversibly transform into quartz in less than 500 Ma (15). Due to the lack of continents and thus influx of silica from continental weathering, a silica cycle on Enceladus may be predominantly controlled by transport from/to the seafloor. As the Enceladus ocean may have existed for hundreds of Ma to several Ga (16, 17), diagenetic reactions in its seafloor might have driven the silica system toward equilibrium and close to the solubility of quartz (log activity of aqueous silica in equilibrium with quartz = -4.64 at 0 °C; data from EQ3/6 (18)). Thus, we set dissolved silica to be the solubility of quartz in our nominal model runs. We also tested the effect of silica level by setting it to be the solubility of amorphous silica (log activity of aqueous silica in equilibrium with amorphous silica = -3.12 at 0 °C; data from EQ3/6 (18)), cristobalite (log activity of aqueous silica in equilibrium with cristobalite = -3.50 at 0 °C; data from EQ3/6 (18)), or chalcedony (log activity of aqueous silica in equilibrium with chalcedony = -4.34 at 0 °C; data from EQ3/6 (18)).

Total P from Enceladus's entire core of assumed CI carbonaceous chondritic composition (19) could provide up to ~100 mmole/kg H_2O if totally released into the ocean. Additional phosphorus may come from cometary volatiles (e.g. Altwegg et al., 2016 (20)), similar to halogens. In this study, we iterated the model and set dissolved phosphate to the solubility of the least soluble P-minerals in the simulated Enceladus ocean water (**Fig. S3**). Thus, our estimates may represent an underestimate of total P level, as reduced inorganic P or organic P, delivered by cometary impacts, could have added more dissolved P to the Enceladus ocean.

The temperature in our model was set to 0 °C in standard runs, representing globally ubiquitous conditions in the ice-covered ocean of Enceladus. However, geochemical evidence suggests the occurrence of hydrothermal activity, likely reaching >50 °C (21). While such activity may be localized (see **Section S5**), it is useful to understand how it could affect the availability of P in the ocean. To evaluate the potential effect of a temperature gradient on P availability, we used our 0 °C result as an input to a heating model which increased the fluid temperature to a higher value (25, 60, or 100 °C). The heating model had no mineral input but was allowed to precipitate out minerals. Therefore, the simulated P level at elevated temperatures may not be any lower than P mineral solubilities in hot fluids.

All of the thermodynamic calculations described above were conducted using the aqueous speciation and mineral solubility code EQ3NR. For the heating model, we used EQ3NR's result (at 0 °C) as an input for EQ6 which simulates aqueous speciation and mineral precipitation that would occur for an increase in temperature of up to 100 °C.

S2. Pressure effect on the model

The pressure in our model is equal to the reference pressure of 1 bar. Due to the coverage of an icy shell and overlying water column, the actual pressure of ocean water inside Enceladus may range from ~20 to ~70 bars depending on depth in the ocean. To examine the pressure effect on the model results, we calculated equilibrium constants (log K_{diss}) of dissolution reactions of major P-minerals (for example, $Ca_5(PO_4)_3F + 3H^+ \rightarrow 5\ Ca^{2+} + 3\ HPO_4^{2-} + F^-$) as a function of pressure at 0 °C. The calculations were performed by the Fortran computer code SUPCRT92b (http://www.dewcommunity.org/resources.html) (22), with thermodynamic properties of minerals from Berman (1988) (23) and apatite minerals from Zhu & Sverjensky (1991) (24). For vivianite, merrillite, struvite, and whitlockite, owing to a lack of mineral density data at both 0 °C and high temperatures, we adopted constant molar volumes of these minerals equal to the values at 25 °C

and 1 bar (**Table S5**). Thus, the effect of pressure (P_{tot}) on Gibbs free energies of formation ($\Delta G_{f,1\rightarrow P}$) of the four minerals can be approximated by

$$\Delta G_{f,1\rightarrow P} = V^{\circ} \times (P_{tot} - 1), \quad \text{(S1)}$$

where V° is taken to be the mineral molar volume (cm^3/mole) at 25 °C and 1 bar. Then, the pressure effect on phosphate mineral solubility can be assessed as antilog ($\frac{(\log K^{P}_{diss} - \log K^{P=1\ bar}_{diss})}{n}$), where *n* designates moles of P atoms released per 1 mole dissolution reaction.

The results show an overall positive effect from pressure on P mineral solubilities at pressures < 80 bars (**Fig. S6**), indicating that our modelling results at 1 bar likely represent a slight underestimate of the equilibrium P concentration in Enceladus's ocean. Pressure has little (a factor of less than 1.5 for most P-minerals) to modest (a factor of 2.3 for struvite) effects on the solubilities of P-minerals. The pressure effect is much smaller than the effects of compositional variations, which can change the results by several orders of magnitude (**Fig. 2; S2, S4 & S5**).

S3. Sensitivity tests

In addition to the standard boundary conditions constrained by Cassini mission data (**Fig. 2; S2 & S3**), we conducted sensitivity tests over a much broader range of environmental factors (fluorine, carbonate, redox state, ammonia, temperature, and silica) that could potentially affect P levels in Enceladus ocean water.

S3.1 Sensitivity to fluorine level

Our results show an overall negative effect of fluorine on P concentration due to the low solubility of F-apatite (**Fig. 2; S2 & S5**). However, fluorine is about 10 times lower in atomic abundance than phosphorus in CI material (**Table S6**); consequently, fluorapatite ($Ca_5(PO_4)_3F$) is not expected to be a predominant sink of P. Apart from fluorapatite and fluorite, fluorine also commonly substitutes for OH in hydrated silicate minerals including micas, amphiboles, and serpentine-group minerals during water-rock reactions (24, 25). If any of these minerals are abundant hosts for F on Enceladus, then there would be even less F available to influence P. Therefore, our estimates in the presence of high fluorine should serve as conservative values for dissolved P in Enceladus ocean water (**Fig. 2; S5**).

S3.2 Sensitivity to carbonate level

Based on analysis of plume ice grains from Enceladus, levels of total carbonate species were inferred to be between 0.01 and 0.1 molal (1). Our results suggest that P levels in the high C case (0.1 molal) are overall higher than in the low C case (0.01 molal) (**Fig. S2, S4 & S5**). This seemingly positive relationship between carbonate and dissolved P levels was further tested and substantiated over a wider range of carbonate concentrations (**Fig. S8**). The positive relationship and the absolute levels of dissolved P are similar to previous observations of certain modern Earth surface waters which displayed a linear correlation between log [total carbonates] and log [total P] (26, 27). These similarities reflect the same general mechanism for P-enrichment, i.e., in the presence of abundant carbonate species at alkaline pH, formation of carbonate minerals suppresses concentrations of key divalent cations (Ca, Mg, Fe) and consequently allows higher solubility of P-minerals. However, unlike Enceladus's ocean, the chemistry of terrestrial alkaline lake waters is further complicated by runoff input, high fluxes of evaporation, and/or precipitation of amorphous precursor minerals (28, 29) reflecting the rapid cycling of elements in the solar-powered surface environment of Earth. Moreover, modern soda lakes are under a strongly oxidizing atmosphere, potentially leading to the oxidation of Fe(II) rather than precipitation of Fe(II)-carbonate/phyllosilicate in anoxic settings (like Enceladus's ocean).

S3.3 Sensitivity to H_2 level

Redox state can directly influence the abundance of P in liquid water by controlling phosphorus speciation because of higher solubilities of solids containing reduced phosphorus, e.g. phosphite P(III) (30), compared with orthophosphate. However, under the inferred redox conditions of Enceladus ocean water, indicated by observed $H_{2,g}$ levels, orthophosphate was found to be the predominantly stable form of P (**Fig. 1 & S1**). In the presence of iron, redox state can also indirectly

affect the availability of P, by precipitating strengite ($Fe(III)PO_4 \cdot 2H_2O$) under oxidizing conditions, or vivianite ($Fe_3(PO_4)_2 \cdot 8H_2O$) under reducing conditions. Under the apparent redox states of Enceladus's ocean, Fe should always be in the form of Fe(II) (31). As a consequence, variation of redox state within present boundary constraints (H_2/CO_2 ratio = 0.5-4.7; Waite et al., 2017 (4)) has minimal effects on levels of oceanic orthophosphate as shown in **Fig. S4 & S5**.

S3.4 Sensitivity to ammonia content

According to INMS data, nitrogen in the ocean of Enceladus is predominantly in the fully reduced form with an N/CO_2 ratio of about 1.5 (4). In the presence of high levels of ammonium (together with other cations), dissolved phosphate can precipitate as ammonium phosphate (e.g., struvite) (32, 33). Indeed, at relatively low pHs (7-7.5), our model shows struvite to be the least soluble (most stable) P-mineral which can maintain dissolved P at somewhat decreased levels (**Fig. 2; S2 & S3**). Furthermore, sensitivity tests of N level (N/CO_2 = 0.15 or 15; corresponding to the low or high N case, respectively) on P level showed that high levels of N would decrease P levels that are controlled by the solubility of struvite (**Fig. S4 & S5**). However, a high NH_4^+ content may not be consistent with CDA data. As an example, there is not a large peak at 18 u in Fig. 1b of Postberg et al., 2009 (1), and mass 18 peaks that can be attributed to NH_4^+-bearing salts have not been seen in other spectra of Type 3 (salt-rich) grains (Khawaja et al., 2019 supplement (34)).

S3.5 Sensitivity to temperature

Due to the fact that neutral pH varies with temperature, P levels at different temperatures were plotted against the reference pH value at 0 °C (for T = 25, 60, or 100 °C; **Fig. S7** shows the starting pH at 0 °C). Our results displayed a negligible effect of temperature on P level in Enceladus ocean water. However, this consideration is most relevant to localized fluids because high-temperature geochemical processes may not dominate the composition of the bulk ocean, assuming elements/aqueous species have low temperature sources of appreciable magnitude (see **Section S5**).

S3.6 Sensitivity to silica concentration

Phosphorus rarely precipitates with silica to form silicate minerals (18 P-Si minerals out of 449 P-minerals; data from http://rruff.info). However, silica level can affect relative stabilities of secondary silicate and carbonate minerals and thus levels of dissolved cations (e.g., Mg, Fe, and Ca). In this way, silica can indirectly influence P level. To examine effects of silica level on P level, we set dissolved silica to be at equilibrium with the most soluble silica solid – amorphous silica. Our results suggest that high silica level has a negative effect on P level at moderately alkaline pHs but a weakly positive or negligible effect at very high pH (**Fig. S9**). These effects are largely due to changing stability relationships between phyllosilicate and carbonate minerals and thus concentrations of Mg and Ca at high dissolved silica. For example, at moderately alkaline pHs (9-10) and very high silica concentration (controlled by solubility of amorphous silica), talc ($Mg_3Si_4O_{10}(OH)_2$, a common phyllosilicate formed by seafloor weathering) is found to be more stable than magnesite ($MgCO_3$) in our model, leading to a lower concentration of magnesium in modeled ocean water. In turn, solubility of calcium is predicted to increase because of solubility control by dolomite ($CaMg(CO_3)_2$). In the presence of F^-, fluorapatite ($Ca_5(PO_4)_3F$) is the least soluble phosphate mineral, whose solubility is very sensitive to calcium concentration and decreases as calcium concentration increases. In the absence of F^-, merrillite ($Ca_{9.5}Mg(PO_4)_7$) is found to be the least soluble phosphate mineral in the case of silica concentration controlled by amorphous silica solubility, instead of vivianite ($Fe_3(PO_4)_2 \cdot 8H_2O$) in other runs with lower silica concentrations. At very high pH of 12, elevation of silica would have a negative effect on calcium concentration due to formation of tremolite ($Ca_2Mg_5Si_8O_{22}(OH)_2$) and thus indirectly favors higher solubility of calcium phosphate minerals (F-apatite in the presence of fluorine; merrillite in the absence of fluorine). Similar to the sensitivity test with fluorine, the results for high silica level may provide a conservative estimate of P levels (but still comparable to or higher than seawater on Earth), because the silica concentration in the bulk ocean is thought to be lower than the solubility of amorphous silica (see **Section S1**).

Hydrothermal activities in Enceladus's core may delivery locally high concentrations of dissolved silica (5, 21) and cause supersaturation with respect to various silica solids in a

hydrothermal plume. To test its effect on P concentration, we performed additional simulations at 5 mM dissolved silica (about 5 times the solubility of amorphous silica at 0 °C and neutral pH). Similar to what we already observed in previous calculations, elevation of silica concentration would decrease the predicted solubility of P by affecting the concentrations of divalent cations (Ca, Mg, Fe) at weakly alkaline pHs (pH < 9; **Fig. S9**). However, at moderately alkaline to high pHs (pH $\geqslant$ 9), increasing $SiO_{2(aq)}$ from amorphous silica solubility to 5 mM has negligible or weakly positive effects on P solubility. We should emphasize that even at high concentration of dissolved silica, the predicted dissolved P concentration could still reach 10^{-7} to 10^{-4} molal at pH between 8.5 to 11 (previously proposed to be relevant to Enceladus ocean water). Moreover, precipitation of amorphous silica could reach equilibrium in days (35, 36), and a hydrothermal plume is likely to be chemically distinct from the global ocean-seafloor system that is expected to govern the abundance of oceanic phosphate (see **Section S5**).

Above, we examined the effects of various environmental factors representing a larger range of possibilities than the observationally constrained nominal conditions (**Fig. 2**). In summary, pH, fluorine, carbonate, ammonia, and silica contents have either positive or negative effects on P levels in Enceladus's ocean water, whereas redox state and temperature have negligible effects. It should be noted that some sensitivity tests (e.g., relatively low or high pHs, high levels of fluorine, carbonate, ammonia, or silica) are likely to provide conservative estimates of P levels, and the actual P level can be expected to be higher than those estimates. Nevertheless, all of the estimates are higher than or close to P levels in modern Earth seawater, suggesting enough P for possible life in the Enceladus ocean.

S4. Potential effects of mineral adsorption

In the phosphorus cycle on modern Earth, seafloor weathering of basalt acts as a net sink of P mainly controlled by surface adsorption onto sedimentary minerals and burial of Ca-P minerals (37–40). The surface adsorption is largely mediated through the uptake of inorganic phosphate by Fe(III)-hydroxide (40, 41). In contrast, Enceladus's ocean water is overall reducing, carbonate-rich, and alkaline. In such ocean water, formation and persistence of Fe(III)-hydroxide is thermodynamically disfavored.

At alkaline pHs, green rust (another known scavenger of phosphate (42)) can form and metastably exist in the presence of reducing seawater with low Fe(III) content (43). However, green rust is not a thermodynamically stable phase and will eventually transform into greenalite (at high silica or low carbonate levels) or siderite (at low silica or high carbonate levels) (43–45). This transformation is more likely to occur in Enceladus's ocean given that its seafloor is likely to be 100s Ma to several Ga old (the relatively low derived density (2400 – 2500 kg/m^3) of its core (46) is consistent with the occurrence of abundant alteration phases, and argues against basaltic volcanism that would rejuvenate the seafloor). It can be expected that such long durations would support mineralogical transformations toward equilibrium (see **Section S1**). Moreover, the surface of green rust will become negatively charged at pH > 8.3 (47) (**Table S7**), which does not favor phosphate adsorption. Thus, adsorption onto $Fe(OH)_x$, including green rust, may not be a significant sink for P in Enceladus's ocean water.

Our geochemical model suggests favorable precipitation of carbonate minerals (calcite, magnesite, siderite, and dolomite) and phyllosilicates (lizardite, greenalite, talc, and tremolite) at Enceladus's seafloor. Surfaces of these minerals will be net negatively charged because their points of zero charge are lower than the inferred pH (8.5 - 11) of Enceladus ocean water (**Table S7**). Phosphate is negatively charged in Enceladus ocean water as well, mainly as HPO_4^{2-}. Thus, the electrostatic repulsion between negatively charged mineral surfaces and HPO_4^{2-} would result in minor uptake of phosphate by mineral adsorption, consistent with various experiments showing decreasing adsorption of phosphate at alkaline pHs (48–51). Moreover, dissolved (bi)carbonate in the Enceladus ocean would decrease phosphate adsorption onto secondary minerals (52). It is notable that at high concentrations of dissolved phosphate above the saturation limit of P-minerals, mineral adsorption might facilitate surface precipitation of P-minerals (53, 54). This effect is already captured by our model by assuming a P level that is in equilibrium with the least soluble P-mineral. Overall, mineral adsorption can be expected to have little if any influence on the present results.

S5. Impact of hydrothermal processes

The geochemical model presented in the main text is a low-temperature model. It is based on the high likelihood of there being an ice-covered (cold) ocean that is in contact with rocks on the ocean floor of Enceladus (55, 56). Low temperature water-rock interaction seems inescapable (8). The role of high temperature processes is less clear as the current observational evidence is indirect (4, 5), and we do not know how tidal heating is distributed between the ice shell and the rocky core (57, 58). Nevertheless, we are motivated to consider the impact of hydrothermal processes on the phosphate concentration in Enceladus's ocean because they could be important.

We construct a simple box model for phosphate in the Enceladus ocean. If there is heterogeneous heat generation or transfer in Enceladus's core, then there could be both low- and high-temperature fluids in the core. This would be similar to the situation at Earth's seafloor, where we can observe high-temperature venting at mid-ocean ridges and low-temperature off-axis fluid circulation (e.g., Campbell et al., 1988 (59); Wheat et al., 2017 (60)). Our box model assumes that low temperature dissolution of phosphate minerals is a source of phosphate to the ocean of Enceladus, while removal of phosphate-bearing ocean water into both low- and high-temperature systems in the rocky core are sinks (note that if high-temperature systems provide an additional source of phosphate, then there would be greater availability of phosphate in Enceladus's ocean than calculated below). The concentration of phosphate (*[P]*) in the ocean is related to the source and sinks by

$$\frac{d[\mathrm{P}]_{\mathrm{oc}}}{dt} = \frac{Q_{\mathrm{LT}}[\mathrm{P}]_{\mathrm{LT}} - Q_{\mathrm{LT}}[\mathrm{P}]_{\mathrm{oc}} - Q_{\mathrm{HT}}[\mathrm{P}]_{\mathrm{oc}}}{m_{\mathrm{oc}}}, \quad \text{(S2)}$$

where Q corresponds to the mass flow rate of water into/out of low temperature (LT) or high temperature (HT) systems in the core, and m_{oc} represents the mass of the ocean. Here, we consider an endmember in which it is assumed that phosphate is completely removed from the fluid during high-temperature circulation.

At steady state, the concentration of phosphate in the ocean will be

$$[\mathrm{P}]_{\mathrm{oc}} = \left(\frac{Q_{\mathrm{LT}}}{Q_{\mathrm{LT}} + Q_{\mathrm{HT}}} \right) [\mathrm{P}]_{\mathrm{LT}} = f_{\mathrm{LT}}[\mathrm{P}]_{\mathrm{LT}} \quad \text{(S3)}$$

This equation shows that $[P]_{oc}$ should be some fraction of the phosphate concentration that is produced in the low temperature system. The latter was already estimated (e.g., **Fig. 2; S2, S4 & S5**). If hydrothermal processes are absent, then the equation collapses to the low temperature solution. When both low- and high-temperature fluid circulation occur, the challenge is to estimate the fraction of the total fluid flux between the ocean and core that is transported by low-temperature fluids only. An Earth analogy may help, in light of the lack of measurements of heat and fluid flow from Enceladus's core, and the likelihood (in our opinion) that these flows will be heterogeneous (not easy to calculate *a priori*) because geological systems are often complex. By extrapolating our knowledge of Earth's seafloor to Europa's, Lowell & DuBose (2005) (61) suggested that fluid circulation could transfer ~50% of the total heat flux, and high-temperature fluids would account for ~10-50% of the advective heat flux. While these numbers were for Europa, we note that Steel et al. (2017) (62) arrived at similar values (34 % and 30%, respectively) for Enceladus, based on the same general approach.

As a possible limiting case that maximizes the influences of hydrothermal processes on Enceladus, we consider a 50/50 partitioning between the amount of heat transferred by high temperature vs. low temperature fluids (calculating relative fluxes of fluids does not require heat flux magnitudes). Using an integrated equation for the relationship between the heat and mass flux (Eq. 34 in Glein et al., 2018 (63)), we find that f_{LT} in **Eq. (S3)** is larger than the corresponding heat flux fraction. This is because a larger quantity of low temperature fluid is required to transfer the same amount of heat as a high temperature fluid. The quantity f_{LT} is close to unity if the high temperature fluid is very hot (e.g., > 200 °C). It decreases as the two fluid temperatures begin to converge, but even at T_{HT} = 100 °C and T_{LT} = 25 °C, the value is still ~ 0.8. We conclude that the concentration of phosphate in the ocean will be determined by the low temperature source, unless fluid-mediated heat transfer on Enceladus is almost entirely dominated by high temperature fluids, which would be much different from what occurs on Earth.

S6. Comparison with previous thermodynamic model for Enceladus

The present geochemical model predicts much higher concentrations of dissolved phosphorus (up to 10^{-2} molal) in Enceladus's ocean than did an earlier model (less than 10^{-10} molal (64, 65). According to Zolotov (2012) (64), ß-whitlockite was the P-mineral that controlled the concentration of aqueous P in that model. We believe that our value for the dissolution equilibrium constant of ß-whitlockite in **Table S3** is representative and particularly relevant to the present problem, as it was pegged to the experimentally determined solubility product (K_{sp}) of $10^{-28.92}$ at 25 °C and 1 bar (66) (in our Enceladus model, there is a slight adjustment to 0 °C that is made using the van't Hoff equation). The solubility product quantifies the following equilibrium

$$Ca_3(PO_4)_2 \rightarrow 3Ca^{2+} + 2PO_4^{3-}. \quad \text{(S4)}$$

The question is what is the solubility product from the earlier model? That model used the GEOCHEQ free energy minimization code (67) to determine water-rock equilibrium. We investigated ß-whitlockite solubility using a copy of the GEOCHEQ code that was given to C. Glein from M. Zolotov, when C. Glein worked at Arizona State University from 2006 – 2012. The GEOCHEQ value of the solubility product was calculated in two ways to verify internal consistency. First, we performed a numerical simulation in which a large amount of ß-whitlockite (1 kg) was reacted with pure water (1 kg) at 25 °C and 1 bar. The solubility product for **Reaction (S4)** can be computed using the equilibrium activities of Ca^{2+} and PO_4^{3-} via

$$K_{sp} = a_{Ca^{2+}}^3 \times a_{PO_4^{3-}}^2. \quad \text{(S5)}$$

Activity values from GEOCHEQ are $a Ca^{2+} = 1.41 \times 10^{-8}$ and $a PO_4^{3-} = 1.94 \times 10^{-14}$, yielding log K_{sp} = -50.98. In a second approach, we calculated the solubility product using standard Gibbs free energy of formation values from the GEOCHEQ database. Those values are -952894 cal/mol for ß-whitlockite, -132120 cal/mol for the calcium cation, and -243500 cal/mol for the phosphate anion. We then computed the solubility product using the relationship

$$\Delta G^{\circ}_{Rxn\ S4} = -RT \times lnK_{sp}, \quad \text{(S6)}$$

where R designates the gas constant (1.987 cal mol^{-1} K^{-1}). From this calculation, we obtained an almost identical log K_{sp} value of −50.97. It is evident that GEOCHEQ treats ß-whitlockite as being far less soluble than it should be based on mineral-solution equilibration experiments (log K_{sp} = −28.92; (66)). This many orders of magnitude difference is the dominant reason why previous thermodynamic modeling of the Enceladus ocean predicted only trace availability of dissolved phosphorus. Indeed, **Fig. S10** shows that using the much more negative log K_{sp} derived from GEOCHEQ data would drastically lower the predicted P concentration in Enceladus's ocean from our modeling approach as well.

S7. Is biological synthesis the most plausible process to achieve a significant extent of phosphoanhydride bond formation in Enceladus's ocean?

To illustrate the thermodynamic potential to form phosphoanhydride (P-O-P) bonds under abiotic conditions, we consider the formation of adenosine triphosphate (ATP) from adenosine diphosphate (ADP) and orthophosphate. This is the most important reaction that is used to transfer energy in life as we know it. The reaction can be represented by

$$ADP^{3-} + HPO_4^{2-} + H^+ \rightarrow ATP^{4-} + H_2O. \quad \text{(S7)}$$

At modeled conditions for Enceladus's ocean (0 °C, 1 bar, pH ~8.5-11), HPO_4^{2-} will be the predominant form of orthophosphate (**Fig. 1**), and the fully deprotonated forms of ADP and ATP would be the predominant forms of these species. The pK_a values of the singly protonated forms, designated as $HADP^{2-}$ and $HATP^{3-}$, were calculated to be 7.26 and 7.66, respectively (68); these values are lower than the inferred ocean pH. Note that this approach neglects metal ion complexing of nucleotides, so it will provide a first-order estimate. The equilibrium constant for **Reaction (S7)** can be written as

$$K_{S7} = \frac{a_{ATP^{4-}} a_{H_2O}}{a_{ADP^{3-}} a_{HPO_4^{2-}} a_{H^+}} = \frac{a_{H_2O}}{a_{HPO_4^{2-}} a_{H^+}} \left(\frac{\gamma_{ATP^{4-}}}{\gamma_{ADP^{3-}}} \right) \left(\frac{m_{ATP^{4-}}}{m_{ADP^{3-}}} \right) = 1.8 , \quad \text{(S8)}$$

where a_i stands for the activity of the ith species, γ_i denotes its activity coefficient, and m_i indicates the molal concentration of the species of interest. The value of the equilibrium constant at 0 °C and 1 bar was computed using the CHNOSZ package (69) with thermodynamic data from (68) and (70).

We can estimate the molar ratio of ATP^{4-}/ADP^{3-} at equilibrium by rearranging **Eq. (S8)**, if values are available for the other quantities in that equation. We obtained values for these quantities by performing aqueous speciation calculations using the SpecE8 app (thermo.com.V8.R6+ database) in The Geochemist's Workbench 2021 (similar to what ref. (8) did). Two cases of the major ion composition were considered: (1) a "salty" case with a chlorinity of 0.2 molal and a concentration of total carbonates of 0.1 molal; and (2) a "dilute" case with a chlorinity of 0.05 molal and a concentration of total carbonates of 0.01 molal (**Table S2**). By varying the concentration of orthophosphate and fixing the pH, we obtained values for the first term on the far right side of **Eq. (S8)**. The second term is more challenging to evaluate because ATP^{4-} and ADP^{3-} are not in the thermodynamic database that was used. Two approaches were taken to help bound the problem. In a first approach, we assumed that the ionic charge dominates the degree of non-ideal behavior of ATP^{4-} and ADP^{3-}, and treated $P_2O_7^{4-}$ and $HP_2O_7^{3-}$ as proxies for them. The latter pyrophosphate species are in the thermodynamic database. Our second approach was simpler – we assumed that the activity coefficient ratio in **Eq. (S8)** can be approximated by unity. This may be reasonable if the rest of the nucleotide structure dominates their solution behavior, so that non-ideal effects tend to cancel out.

We find that the equilibrium concentrations of pyrophosphate species are much lower than those of orthophosphate species (**Fig. S13**), and ATP would also be many orders of magnitude lower in concentration than ADP (**Fig. S14**), if these species equilibrated under our modeled conditions for Enceladus's ocean, where a very conservative upper limit for [P] would be ~0.1 molal (**Fig. S8**). Comparison of **Figs. S13** and **S14** shows that the nature of the species that contains a phosphoanhydride bond has an important effect on exactly where the equilibrium lies. However, even for the more favorable case of pyrophosphate formation from a relatively high concentration (100 mmolal) of orthophosphate, the maximum equilibrium concentration of pyrophosphate species was computed to be no higher than ~30 µmolal. Although these are just two examples, our quantification is consistent with the common rule of thumb that it is difficult to form phosphoanhydride bonds in cold water. In general terms, the strongly unfavorable thermodynamic potential for the conversion of more than a miniscule amount of ADP to ATP in Enceladus's ocean implies that larger ratios of ATP/ADP (or analogous pairs of species) would require energy input that is directed in the forward direction of **Reaction (S7)**. Such constructive use of energy is a hallmark of life; thus, life would likely be implicated if this type of disequilibrium were found in samples from Enceladus's ocean.

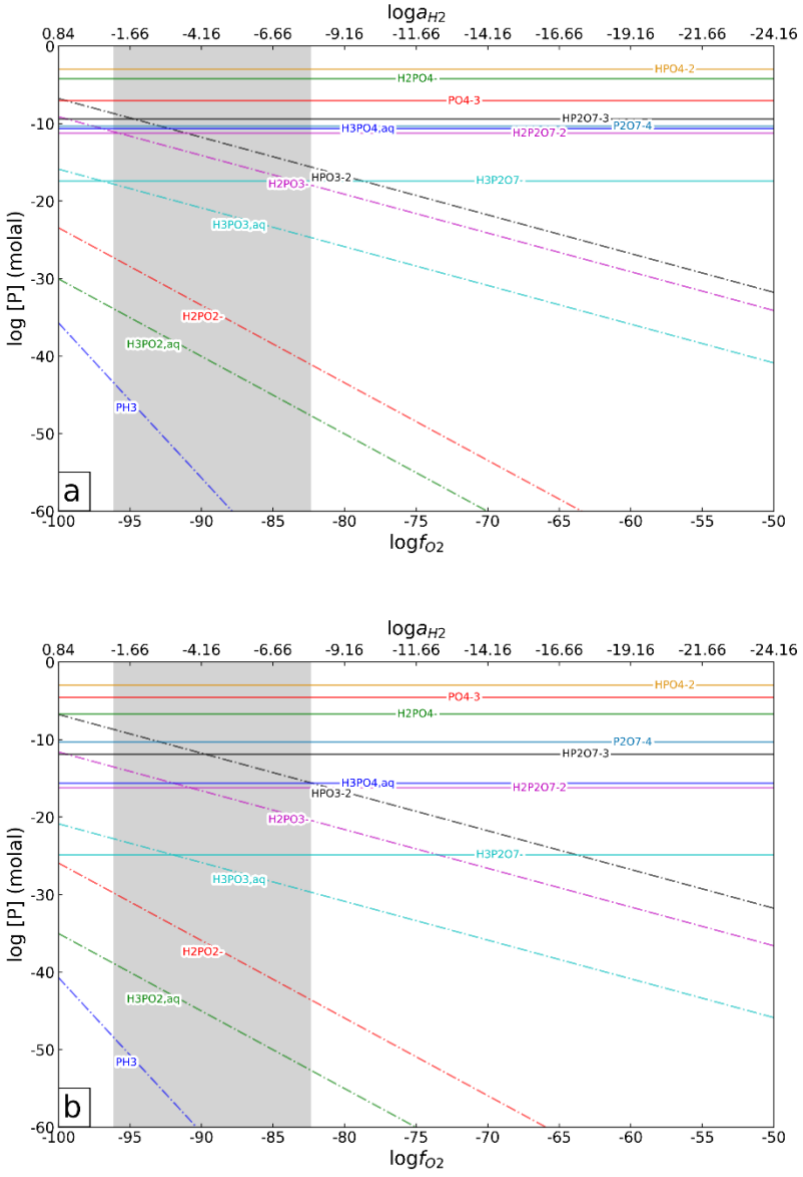

Fig. S1. Calculated equilibrium molal concentrations of aqueous P species as a function of ocean oxidation state (log $fO_{2,g}$; in bars) and pH for 1 mmolal total P at 0 °C and 70 bars, and (A) pH = 8.5 or (B) pH = 11, corresponding to the lower and upper ends of the constrained pH range of Enceladus ocean water, respectively. Thermodynamic properties for aqueous P species were compiled from the literature and are reported in **Table S1**. The shaded region represents inferred redox states of the Enceladus ocean: right limit calculated from a($H_{2,aq}$) of Enceladus ocean water (63); left limit assuming p($H_{2,g}$) equal to seafloor pressure (70 bars). Solid and dashed-dotted lines display levels of phosphates (+V) and reduced phosphorus (+III, +I, and -III), respectively.

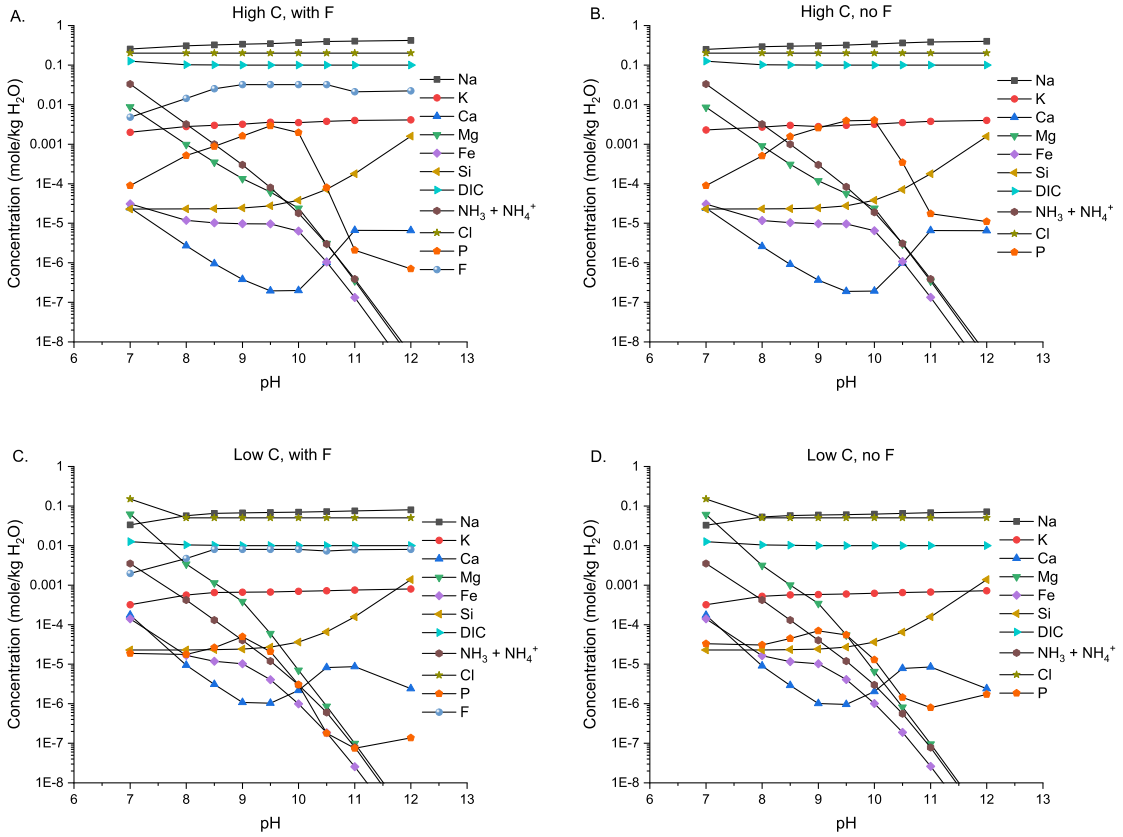

Fig. S2. Simulated equilibrium water chemistry under various nominal conditions of Enceladus's ocean (see **Table S2** for detailed settings) at 0 °C. DIC = Dissolved Inorganic Carbon (i.e., $CO_{2,aq}$ + HCO_3^- + CO_3^{2-}). [C] denotes the total concentration of carbonate ions: HCO_3^- + CO_3^{2-}. The system contains fluorine in the left panels, and fluorine is not included in the right panels.

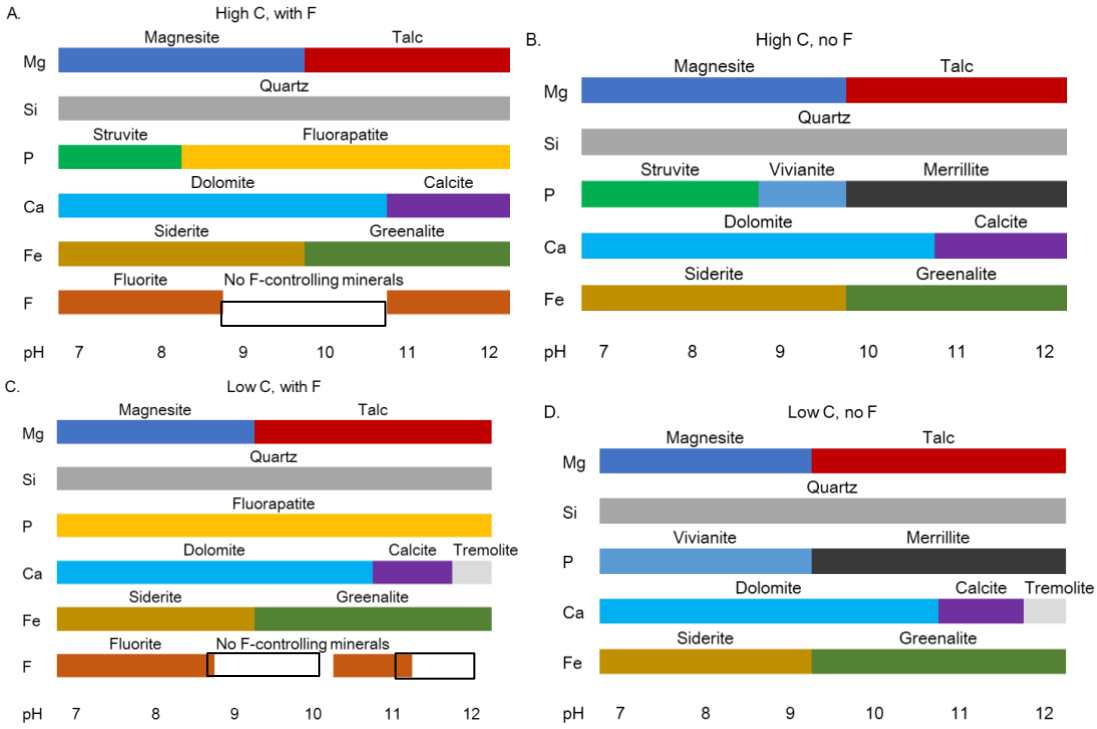

Fig. S3. Simulated saturated mineralogy on the seafloor under various nominal conditions of Enceladus's ocean (see **Table S2** for detailed settings) at 0 °C. [C] denotes the total concentration of carbonate ions: HCO_3^- + CO_3^{2-}. The system contains fluorine in the left panels, and fluorine is not included in the right panels.

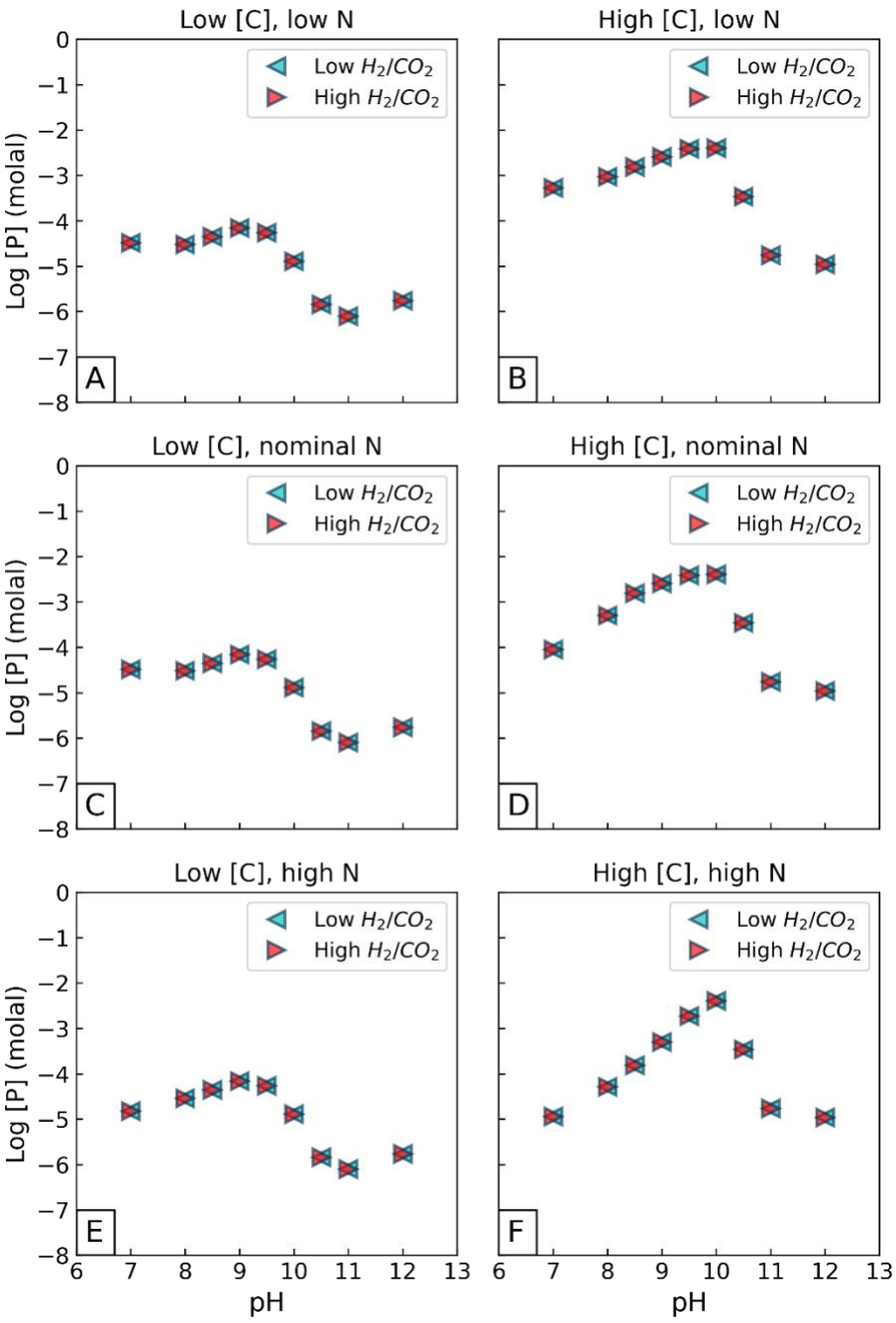

Fig. S4. Concentration of dissolved phosphate under various boundary conditions of Enceladus's ocean (see **Table S2** for detailed settings of A-F) at 0 °C. Fluorine is not included in this model. [C] denotes the total concentration of carbonate ions: HCO_3^- + CO_3^{2-}, [N] denotes the total concentration of $NH_{3,aq}$ and NH_4^+, and H_2/CO_2 denotes the concentration ratio of dissolved H_2 and CO_2.

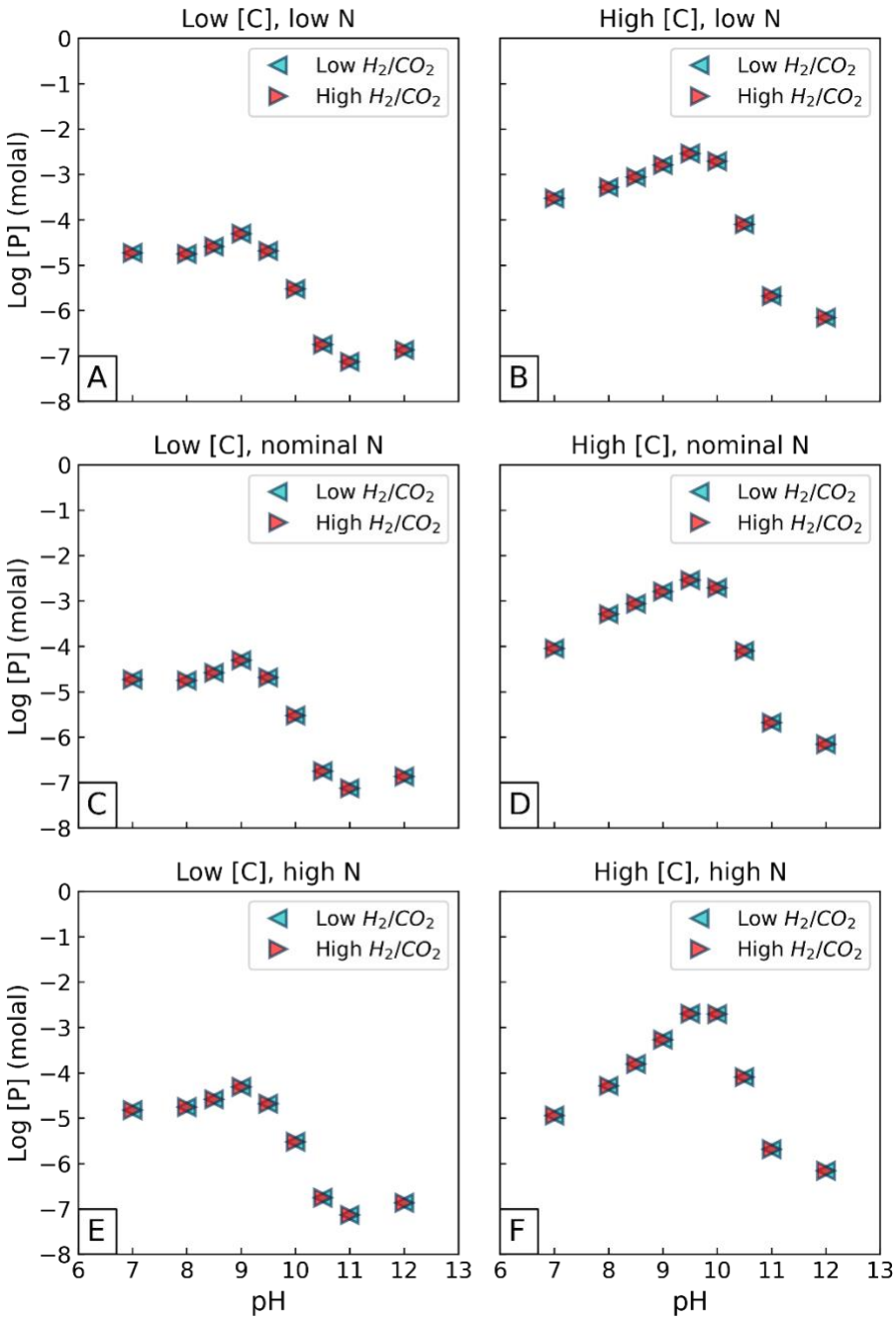

Fig. S5. Concentration of dissolved phosphate under various boundary conditions of Enceladus's ocean (see **Table S2** for detailed settings of A-F) at 0 °C. Fluorine is included in this model by assuming that its concentration is the lower value between the solubility of fluorite (the least soluble F-mineral in the system), and the abundance of F in Enceladus's ocean that would result from the ocean having a similar F/Cl ratio as CI chondrites (see **Section S1**). [C] denotes the total concentration of carbonate ions: HCO_3^- + CO_3^{2-}, [N] denotes the total concentration of $NH_{3,aq}$ and NH_4^+, and H_2/CO_2 denotes the concentration ratio of dissolved H_2 and CO_2.

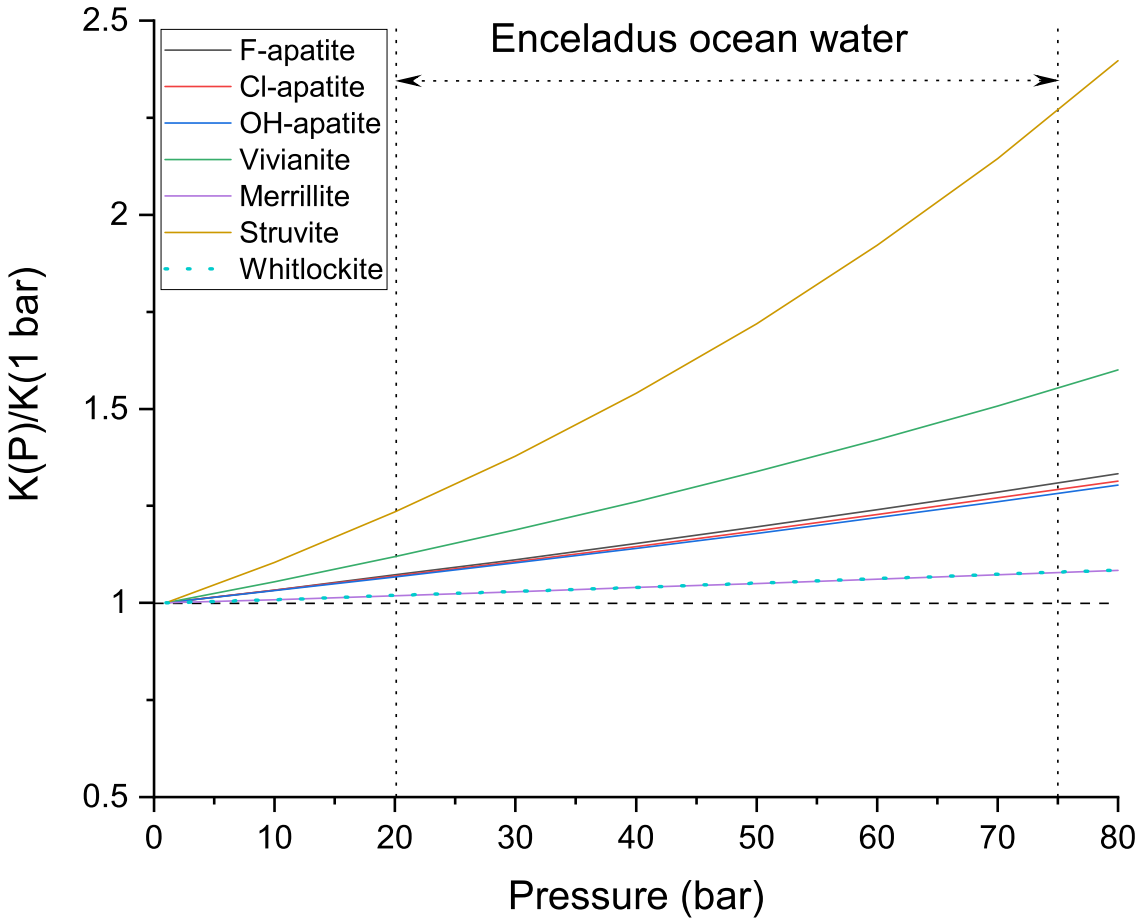

Fig. S6. Pressure effect on the solubilities of P-minerals. *K(P)* represents the equilibrium constant of dissolving a P-mineral to release 1 mole HPO_4^{2-} at different pressures. *K(P)*/*K(1 bar)* shows the ratio of equilibrium constant of reactions involving the noted minerals (per mole of HPO_4^{2-} formed) relative to the equilibrium constant at one bar, *K(1 bar)*. The horizontal dashed line shows where *K(P)*/*K(1 bar)* = 1: above this line, pressure produces a positive effect on the solubility and below this line, the solubility decreases with increasing pressure. Vertical dotted lines encompass the pressure range in Enceladus's ocean. Whitlockite is shown with a dotted curve to help distinguish it from merrillite.

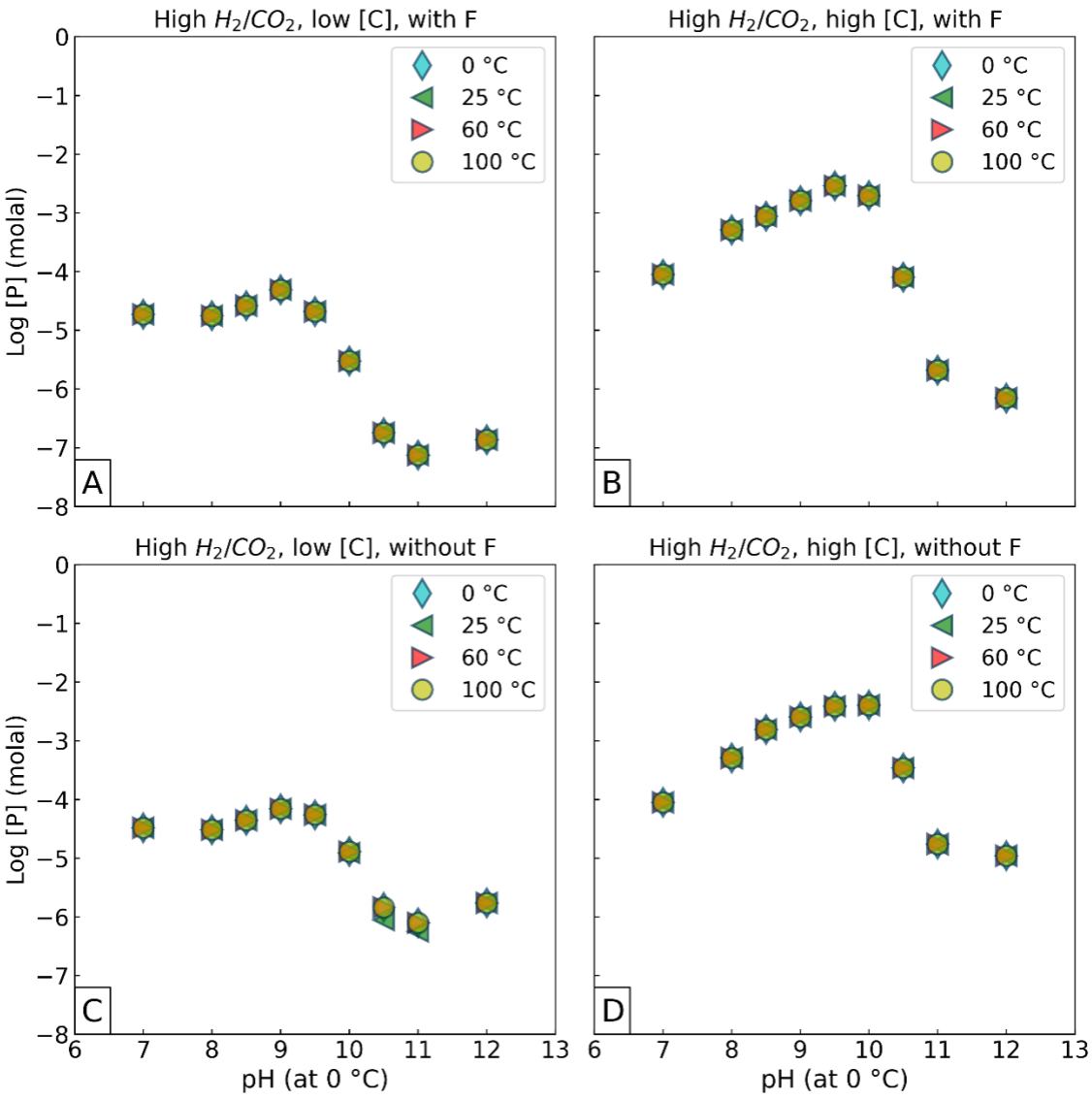

Fig. S7. Sensitivity tests of how heating of Enceladus ocean water affects dissolved phosphate levels. In these tests, the $(NH_3+NH_4^+)/CO_2$ molar ratio is assumed to be 1.5 (nominal condition). [C] denotes the total concentration of carbonate ions: HCO_3^- + CO_3^{2-}, and H_2/CO_2 denotes the concentration ratio of dissolved H_2 and CO_2. The system contains fluorine in the top panels, and fluorine is not included in the bottom panels.

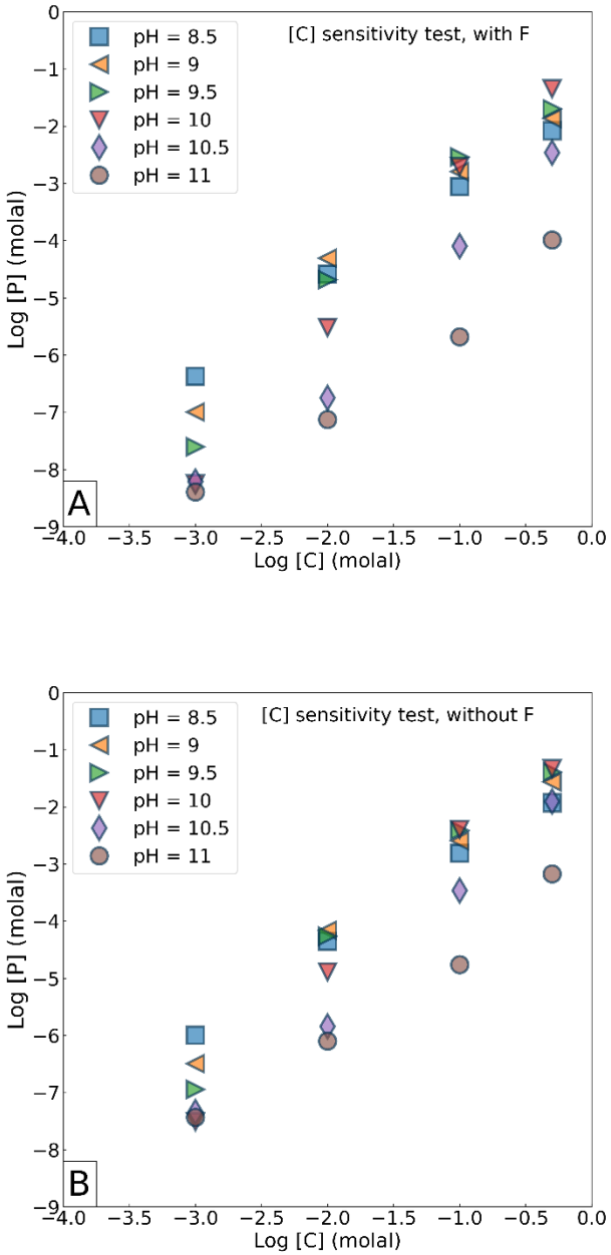

Fig. S8. Sensitivity tests of dissolved carbonate effects on dissolved phosphate levels at 0 °C. Here, it is assumed that the H_2/CO_2 molar ratio is 4.7 and the $(NH_3+NH_4^+)/CO_2$ molar ratio is 1.5 (nominal conditions). The system contains fluorine in the top panel, and fluorine is not included in the bottom panel.

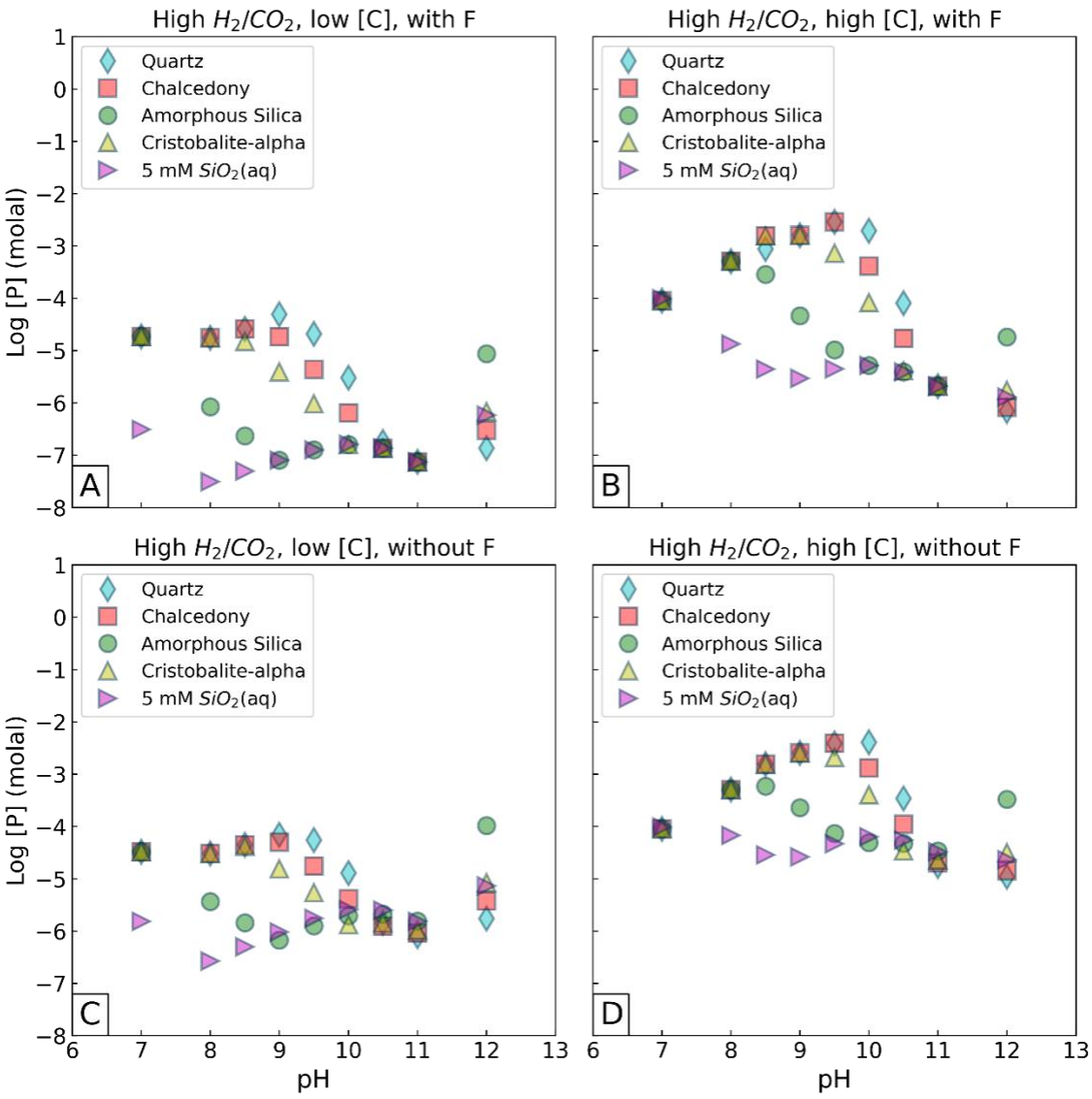

Fig. S9. Sensitivity tests showing how allowing various silica minerals to control the silica concentration as well as an arbitrarily high SiO_2(aq) concentration of 5 mM affect dissolved phosphate levels at 0 °C. The $(NH_3+NH_4^+)/CO_2$ molar ratio is assumed to be 1.5 (nominal condition). [C] denotes the total concentration of carbonate ions: HCO_3^- + CO_3^{2-}, and H_2/CO_2 denotes the concentration ratio of dissolved H_2 and CO_2. The system contains fluorine in the top panels, and fluorine is not included in the bottom panels.

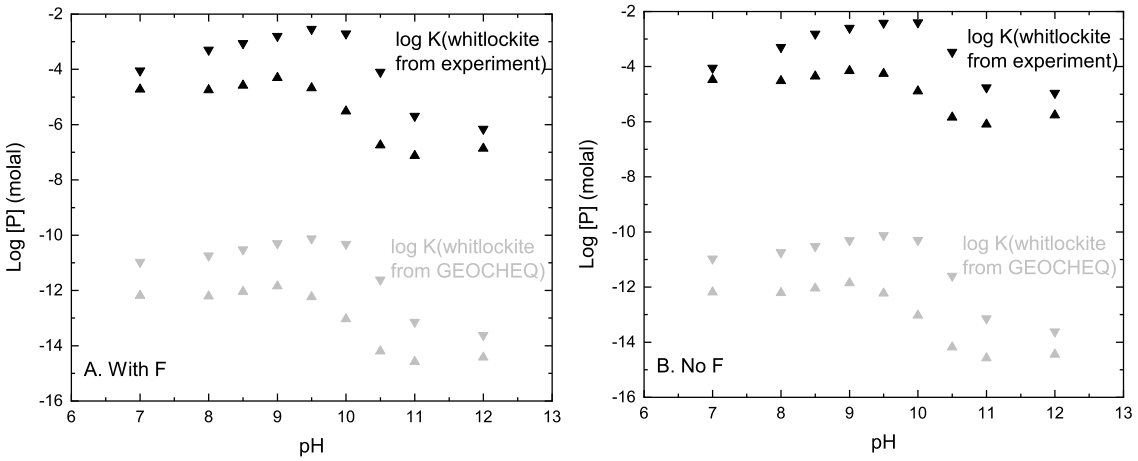

Fig. S10. Comparison of our predicted P concentrations in nominal model runs (**Table S2**; **Fig. 2**) with the results obtained by adopting log K_{sp} (for whitlockite) derived from GEOCHEQ thermodynamic data (64, 65). The system contains fluorine in the left panel, and fluorine is not included in the right panel.

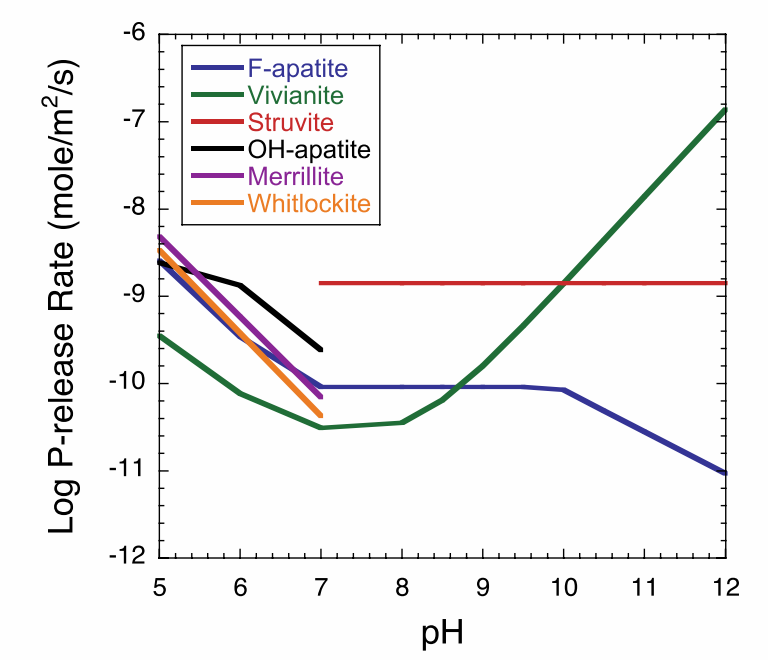

Fig. S11. Release rates of P from dissolution of common P-minerals under various pH conditions in previous studies at 25 °C. See **Table S5** for data sources.

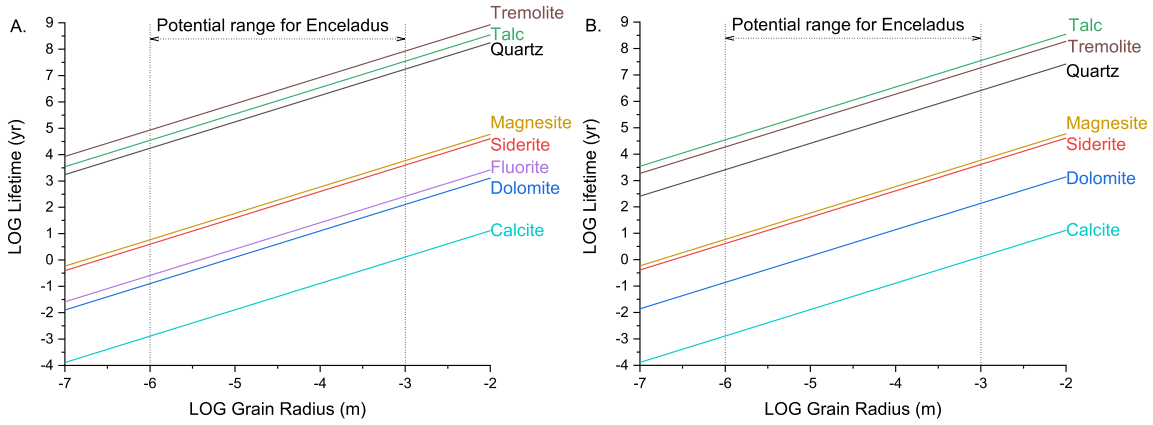

Fig. S12. Lifetime of mineral dissolution: A. pH = 8.5; B. pH = 11. Lifetime is defined as the duration for total dissolution of round crystals (71) at the given pH and 0 °C with kinetic dissolution rates for quartz (72), fluorite (73, 74), calcite (75), dolomite (72), magnesite (75), talc (76), tremolite (77), and siderite (72). Due to lack of kinetic data for fluorite dissolution at pH = 11, its lifetime could not be estimated at this pH.

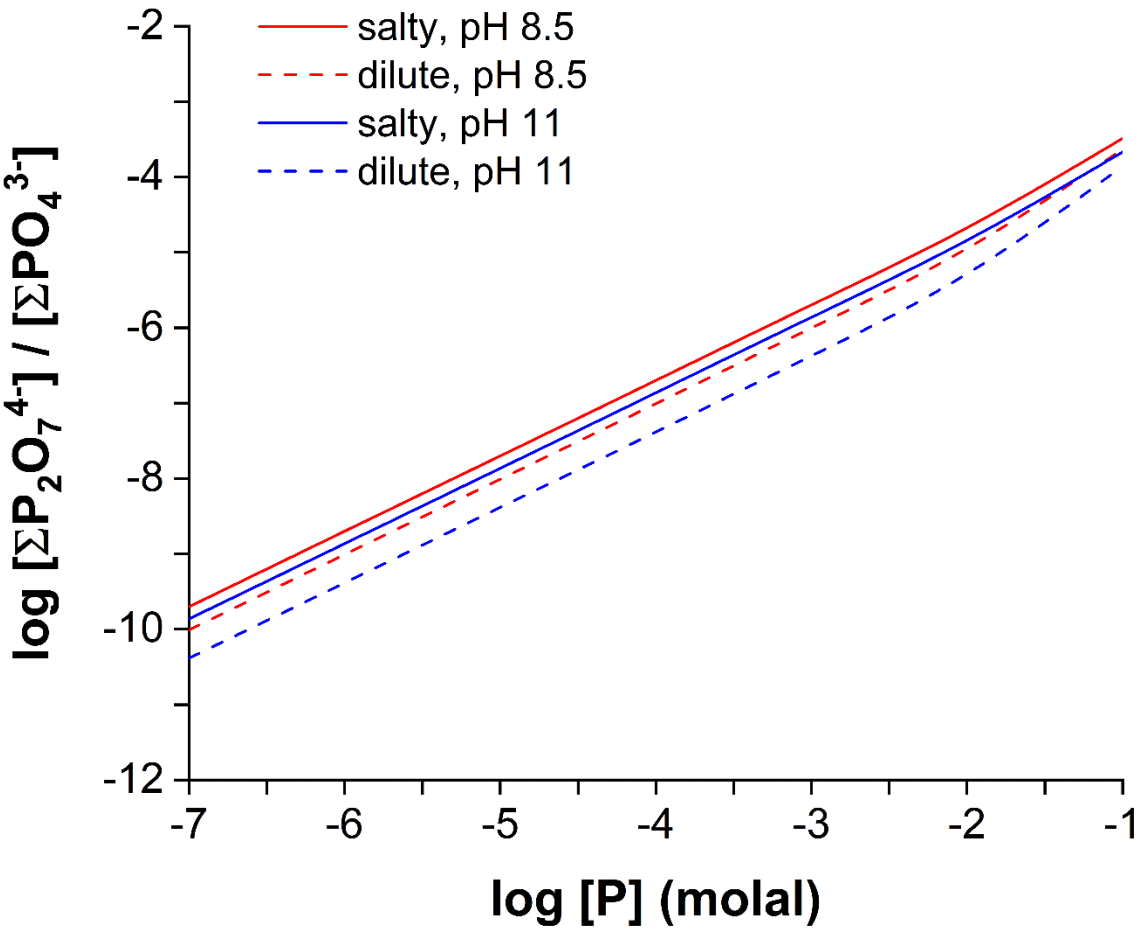

Fig. S13. Equilibrium concentration ratio of pyrophosphate species ($\Sigma P_2O_7^{4-}$ = $P_2O_7^{4-}$ + $HP_2O_7^{3-}$ + $H_2P_2O_7^{2-}$ + $H_3P_2O_7^{-}$ + $H_4P_2O_{7,aq}$) to orthophosphate species (ΣPO_4^{3-} = PO_4^{3-} + HPO_4^{2-} + $H_2PO_4^{-}$ + $H_3PO_{4,aq}$) as a function of the concentration of total phosphate and other geochemical conditions in Enceladus's ocean at 0 °C and 1 bar. Colored lines indicate the effects of pH over a previously inferred range, and solid vs. dashed lines show how the range of major salt concentrations (NaCl, $NaHCO_3$/Na_2CO_3; **Table S2**) affects the thermodynamic potential to produce pyrophosphate from orthophosphate.

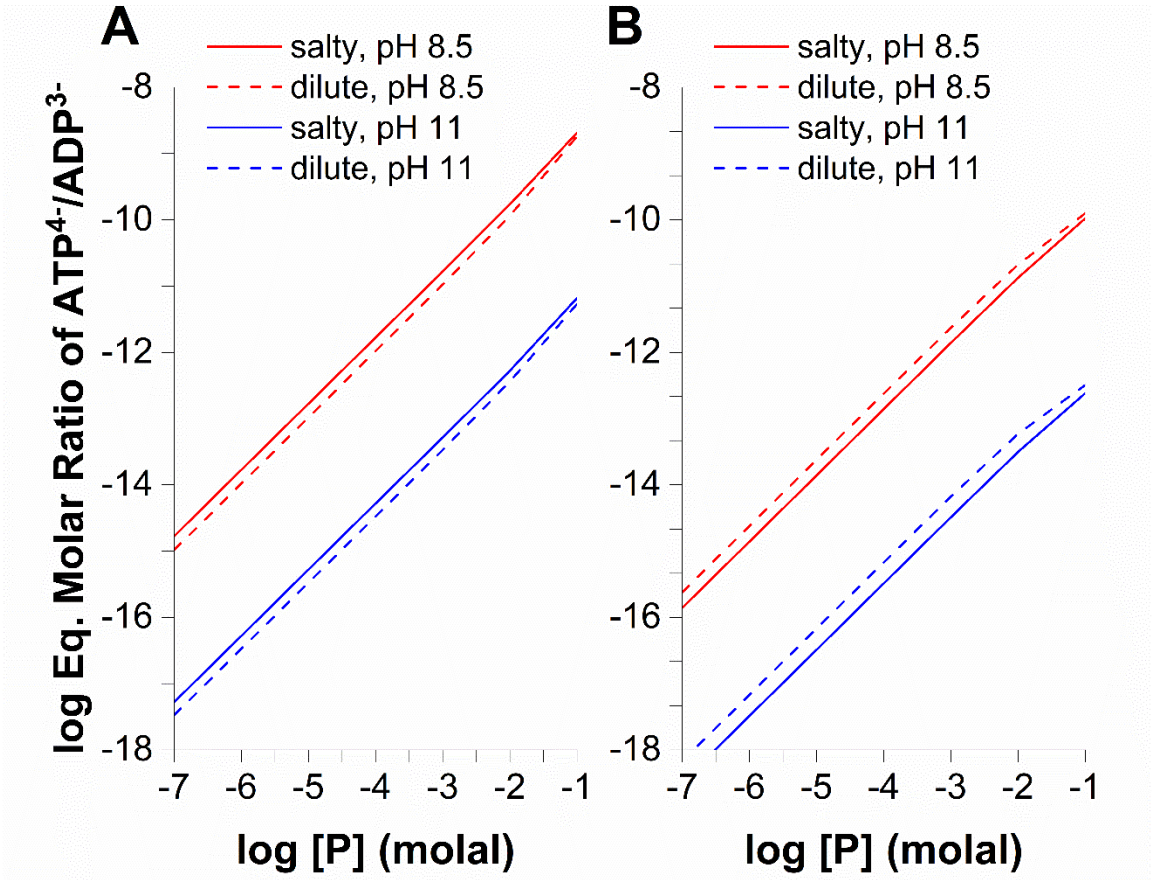

Fig. S14. Equilibrium molar ratio of adenosine triphosphate (ATP, fully deprotonated) to adenosine diphosphate (ADP, fully deprotonated) as a function of the concentration of total phosphate and other geochemical conditions in Enceladus's ocean at 0 °C and 1 bar. In (A), the activity coefficients of $P_2O_7^{4-}$ and $HP_2O_7^{3-}$ from speciation calculations (see **Section S7**) are used as proxies for those of ATP^{4-} and ADP^{3-}, respectively. In (B), the ATP^{4-}/ADP^{3-} activity coefficient ratio is assumed to be unity. Colored lines indicate the effects of pH over a previously inferred range, and solid vs. dashed lines show how the range of major salt concentrations (NaCl, $NaHCO_3/Na_2CO_3$; **Table S2**) affects the thermodynamic potential to produce ATP from ADP and orthophosphate.

Table S1. Thermodynamic properties of aqueous phosphorus species used in the Deep Earth Water (DEW) model to generate the equilibrium speciation diagram (**Fig. 1**).

Species		$\Delta G_f^{\circ\,a,f}$	$\Delta H_f^{\circ\,b,f}$	$S^{o\,c,f}$	$V^{o\,d,f}$	$C_p^{o\,e,f}$	$a_1 \times 10$	$a_2 \times 10^{-2}$	a_3	$a_4 \times 10^{-4}$	c_1	$c_2 \times 10^{-4}$	$\omega \times 10^{-5}$
Formula	Valence	cal mol^{-1}	cal mol^{-1}	cal mol^{-1} K^{-1}	cm^3 mol^{-1}	cal mol^{-1} K^{-1}	cal mol^{-1} bar^{-1}	cal mol^{-1}	cal K mol^{-1} bar^{-1}	cal K mol^{-1}	cal mol^{-1} K^{-1}	cal K mol^{-1}	cal mol^{-1}
$PH_{3,aq}$	-III	6060	-2680	27.4	24.4	50.5	6.2	1.6	3.5	-2.8	33.9	7.3	-0.2
$H_3PO_{2(aq)}$	+I	-125100	-145600	36.9	35.4	14.1	8.3	3.6	1.8	-2.9	12.4	-0.2	-0.2
$H_2PO_2^-$	+I	-122400	-146700	24.1	22.0	-7.0	6.4	1.8	3.3	-2.9	13.7	-4.5	1.3
$H_3PO_{3(aq)}$	+III	-204800	-230600	43.6	19.1	25.1	5.1	0.5	4.4	-2.8	17.9	2.1	-0.3
$H_2PO_3^-$	+III	-202350	-231700	31.7	14.7	5.5	4.9	0.4	4.5	-2.8	20.0	-1.9	1.1
HPO_3^{2-}	+III	-194000	-231600	4.0	4.5	-40.2	3.9	-0.6	5.3	-2.8	11.7	-11.2	3.2
$H_3PO_{4(aq)}$	+V	-273100	-307920	38.0	48.1	23.6	10.8	6.0	-0.2	-3.0	18.0	1.8	-0.2
$H_2PO_4^-$	+V	-270140	-309820	21.6	31.3	-7.0	8.2	3.5	1.9	-2.9	14.0	-4.5	1.3
HPO_4^{2-}	+V	-260310	-308815	-8.0	5.4	-58.3	4.2	-0.3	5.1	-2.8	2.7	-14.9	3.3
PO_4^{3-}	+V	-243500	-305300	-53.0	-30.6	-124.6	-1.2	-7.3	9.6	-2.5	-15.2	-28.4	5.6
$P_2O_7^{4-}$	+V	-458700	-542800	-28.0	21.7	-139.1	7.1	9.5	2.0	-3.2	-11.7	-31.4	6.9
$HP_2O_7^{3-}$	+V	-471400	-543700.	11.0	36.5	-28.7	8.3	12.6	0.8	-3.3	32.2	-8.9	4.6
$H_2P_2O_7^{2-}$	+V	-480400	-544600	39.0	47.1	17.6	9.1	14.4	0.1	-3.4	40.6	0.6	2.6

[a]Standard Gibbs free energy of formation at 25 °C and 1 bar; [b]standard enthalpy of formation; [c]standard partial molal entropy; [d]standard partial molal volume; [e]standard partial molal heat capacity; [f]thermodynamic properties (G, H, S, V, C_p) of $PH_{3,aq}$ come from Schulte et al. (2001) (78) and other species from Shock et al. (1997) (70), with a_1-a_4, c_1-c_2 and ω parameters for the revised Helgeson-Kirkham-Flowers equations of state that are estimated using the DEW methodology (Sverjensky et al., 2014) (79).

Table S2. Model assumptions for Enceladus ocean water chemistry simulations.

Element	Basis for assumption
Na	Charge balance (1, 63)
K	0.01 × c(Na^+) (1, 63)
Cl[a]	0.2 molal at high $CO_{2,aq}$ case; 0.05 molal at low $CO_{2,aq}$ case (1, 63)
Ca	Minimum solubility of secondary Ca-minerals (e.g., dolomite, calcite, aragonite, or tremolite)
F	Lower value between solubility of fluorite or $(F/Cl)_{solar}$ × c(Cl^- in Enceladus ocean water) in the case of F-presence
Mg	Minimum solubility of secondary Mg-minerals (e.g., magnesite, talc)
Fe	Minimum solubility of secondary Fe-minerals (e.g. siderite, greenalite, goethite, hematite, magnetite)
Si	Minimum solubility of quartz, chalcedony, cristobalite, or amorphous silica
P	Minimum solubility of P-minerals (e.g., apatite, vivianite, struvite, merrillite, etc., see **Table S3**)
Total carbonate species[b]	0.1 molal for high C case; 0.01 molal for low C case (1, 63)
$H_{2,aq}$[c]	$H_{2,aq}/CO_{2,aq}$ = 4.7 for high H_2 case; $H_{2,aq}/CO_{2,aq}$ = 0.5 for low H_2 case (4, 63)
Total ammonia[d]	$\Sigma NH_3/CO_{2,aq}$ = 0.15, 1.5, or 15, representing low, nominal, or high N case. Nominal value (1.5) is taken directly from plume gas data (4).

[a] Based on the observational constraint being the carbonates/chloride ratio, and the fact that the concentration of CO_2 increases with an increase in total carbonates concentration at fixed pH; [b] total carbonate species = [CO_3^{2-}] + [HCO_3^-]; [c]H_2 activity estimated here should represent an upper bound due to the condensation of $CO_{2,g}$ of unknown extent at the surface of the tiger stripe fractures. This effect is expected to increase the molar ratio of H_2/CO_2 in the plume gas relative to the ocean (80). [d]The high N case could be representative of the ocean if NH_3 undergoes significant freeze out from the plume gas relative to CO_2. A low N case is also considered in case some NH_3 that was detected by INMS was non-native to the plume and produced by thermally induced decomposition of N-bearing organics inside INMS (81). At least some native plume NH_3 is indicated by the independent detection of plume-derived nitrogen ions in Saturn's inner magnetosphere by the Cassini Plasma Spectrometer (82).

Table S3. Aqueous phosphate species and phosphate minerals included in the EQ3 database.

Aqueous species	$H_3PO_{4,aq}$; $H_2PO_4^-$; HPO_4^{2-}; PO_4^{3-}; $H_2P_2O_7^{2-}$; $HP_2O_7^{3-}$; $P_2O_7^{4-}$; $CaH_2PO_4^+$; $CaHPO_{4,aq}$; $CaPO_4^-$; $Fe(II)H_2PO_4^+$; $Fe(III)H_2PO_4^{2+}$; $Fe(II)HPO_{4,aq}$; $Fe(III)HPO_4^+$; $MgHPO_{4,aq}$; $MgH_2PO_4^+$; $Mg(HPO_4)_2^{2-}$; $MgPO_4^-$; $NaPO_4^{2-}$; $Na_2PO_4^-$; $NaHPO_4^-$; $Na_2HPO_{4,aq}$			
Mineral	Chemical formula	Dissolution reaction	Log K[a]	ΔH_r[a] (kJ/mole)
Fluorapatite	$Ca_5(PO_4)_3F$	$Ca_5(PO_4)_3F + 3H^+ \rightarrow 5Ca^{2+} + 3HPO_4^{2-} + F^-$	-22.8[b]	-104[b]
Hydroxylapatite	$Ca_5(PO_4)_3OH$	$Ca_5(PO_4)_3OH + 4H^+ \rightarrow 5Ca^{2+} + 3HPO_4^{2-} + H_2O$	-5.11[b]	-183[b]
Chlorapatite	$Ca_5(PO_4)_3Cl$	$Ca_5(PO_4)_3Cl + 3H^+ \rightarrow 5Ca^{2+} + 3HPO_4^{2-} + Cl^-$	-9.60[b]	-161[b]
ß-Whitlockite	$Ca_3(PO_4)_2$	$Ca_3(PO_4)_2 + 2H^+ \rightarrow 3Ca^{2+} + 2HPO_4^{2-}$	-4.28[c]	-84.6[c]
Whitlockite	$Ca_9Mg(HPO_4)(PO_4)_6$	$Ca_9Mg(HPO_4)(PO_4)_6 + 6H^+ \rightarrow 9Ca^{2+} + Mg^{2+} + 7HPO_4^{2-}$	-39[d]	-393[e]
Merrillite	$Ca_{9.5}Mg(PO_4)_7$	$Ca_{9.5}Mg(PO_4)_7 + 7H^+ \rightarrow 9.5Ca^{2+} + Mg^{2+} + 7HPO_4^{2-}$	-39[d]	-401[e]
Calcium hydrogen phosphate	$CaHPO_4$	$CaHPO_4 \rightarrow Ca^{2+} + HPO_4^{2-}$	-6.9[f]	-17.2[f]
Vivianite	$Fe_3(PO_4)_2 \cdot 8H_2O$	$Fe_3(PO_4)_2 \cdot 8H_2O + 2H^+ \rightarrow 3Fe^{2+} + 2HPO_4^{2-} + 8H_2O$	-11.1[g]	-24.3[g]
Newberyite	$MgHPO_4 \cdot 3H_2O$	$MgHPO_4 \cdot 3H_2O \rightarrow Mg^{2+} + HPO_4^{2-} + 3H_2O$	-5.83[h]	-27.9[e]
Bobierrite	$Mg_3(PO_4)_2 \cdot 8H_2O$	$Mg_3(PO_4)_2 \cdot 8H_2O + 2H^+ \rightarrow 3Mg^{2+} + 2HPO_4^{2-} + 8H_2O$	-0.51[i]	-69.3[e]
K-struvite	$KMgPO_4 \cdot 6H_2O$	$KMgPO_4 \cdot 6H_2O + H^+ \rightarrow K^+ + Mg^{2+} + HPO_4^{2-} + 6H_2O$	1.73[i]	-0.89[j]
Na-struvite	$NaMgPO_4 \cdot 7H_2O$	$NaMgPO_4 \cdot 7H_2O + H^+ \rightarrow Na^+ + Mg^{2+} + HPO_4^{2-} + 7H_2O$	0.76[k]	11.5[e]
Brushite	$Ca(HPO_4) \cdot 2H_2O$	$Ca(HPO_4) \cdot 2H_2O \rightarrow Ca^{2+} + HPO_4^{2-} + 2H_2O$	-6.56[l]	0.17[l]
Octacalcium phosphate	$Ca_4H(PO_4)_3 \cdot 2.5H_2O$	$Ca_4H(PO_4)_3 \cdot 2.5H_2O + 2H^+ \rightarrow 4Ca^{2+} + 3HPO_4^{2-} + 2.5H_2O$	-11.3[m]	-123[e]
Struvite	$NH_4MgPO_4 \cdot 6H_2O$	$NH_4MgPO_4 \cdot 6H_2O + H^+ \rightarrow Mg^{2+} + NH_4^+ + HPO_4^{2-} + 6H_2O$	-13.4[n]	84.0[n]
Strengite	$Fe(PO_4) \cdot 2H_2O$	$Fe(PO_4) \cdot 2H_2O + H^+ \rightarrow Fe^{3+} + HPO_4^{2-} + 2H_2O$	-14.1[o]	-24.3[p]
Francolite	$Ca_{10}(PO_4)_{5.5}(CO_3)_{0.5}F_{2.5}$	$Ca_{10}(PO_4)_{5.5}(CO_3)_{0.5}F_{2.5} + 5.5H^+ \rightarrow 10Ca^{2+} + 5.5HPO_4^{2-} + 0.5CO_3^{2-} + 2.5F^-$	-23.3[q]	No data

[a]Data at 25 °C and 1 bar; [b]calculated by SUPCRT92b with $\Delta G_{f,mineral}$ from Zhu & Sverjensky (1991)(24); [c]Gregory et al. (1974) (66); [d]Adcock et al. (2013)(83); [e]calculated using $\Delta H_{f,mineral}$ that was estimated by the method proposed in Iglesia (2009)(84); [f]McDowell et al. (1971)(85); [g]Al-Borno & Tomson (1994)(86); [h]Racz & Soper (1968)(87); [i]Taylor et al. (1963)(88); [j]Luff & Reed (1980)(89); [k]Xu et al. (2015)(90); [l]Patel et al. (1974)(91); [m]Tung et al. (1988)(92); [n]Bhuiyan et al. (2007)(93); [o]Nriagu (1972)(94); [p]Egan et al. (1961)(95); [q]Vieillard (1978)(96).

Table S4. Comparison of equilibrium minerals in our simulations and minerals in chondrites that were altered by aqueous fluids. Note that we made the common approximation in geochemical modeling of treating minerals as pure endmembers, while chondritic minerals often exist as more complex solid solutions.

Element	Mineral	Chemical formula	This study	Chondrites[a]
Si	Quartz	SiO_2	√	√
F	Fluorite	CaF_2	√	√
Ca	Calcite	$CaCO_3$	√	√
	Dolomite	$CaMg(CO_3)_2$	√	√
Mg	Magnesite	$MgCO_3$	√	√
	Talc	$Mg_3Si_4O_{10}(OH)_2$	√	√
	Tremolite	$Ca_2Mg_5Si_8O_{22}(OH)_2$	√	√
Fe	Siderite	$FeCO_3$	√	√
	Greenalite	$Fe_3Si_2O_5(OH)_4$	√	√
P	Apatite	$Ca_5(PO_4)_3(OH,Cl,F)$	√	√
	Merrillite	$Ca_{9.5}Mg(PO_4)_7$	√	√
	Vivianite	$Fe_3(PO_4)_2*8H_2O$	√	√
	Struvite	$MgNH_4PO_4*6H_2O$	√	(√)[b]

[a]Observed as secondary minerals produced by aqueous alteration (6, 97–100); [b]Likely to be present but not observed in chondrites probably due to how easily struvite can be converted to other phosphates (via loss of ammonium in low-N aqueous solutions, or thermal decomposition to form Mg-phosphate or Ca-phosphate at elevated temperatures) (101).

Table S5. Dissolution kinetics of phosphate minerals.

Mineral	Chemical formula	Molar mass (g/mole)	Density (g/cm^3)[a]	pH	Dissolution rate ($mole/m^2/s$)[b]	Activation energy (kJ/mole)	Reference(s)
F-apatite	$Ca_5(PO_4)_3F$	504.3	3.2	3-7 7-10 > 10	log R = -0.87 × pH - 5.0 Constant (-10.8) log R = -0.48 × pH - 6.1	46	Chairat et al. (2007) (102); Harouiya et al. (2007) (103)
OH-apatite	$Ca_5(PO_4)_3(OH)$	502.3	3.2	< 7	$R = -8.9 \times 10^{-10} \times \frac{9.96 \times 10^5 \times a_{H^+}}{1 + 9.96 \times 10^5 \times a_{H^+}}$	No data	Oliva et al. (2012) (104)
Vivianite	$Fe_3(PO_4)_2 \cdot 8H_2O$	501.6	2.7	2-10	$R = 1.18 \times 10^{-10} a_{H^+}^{0.77} + 1 \times 10^{-15} + 6.92 \times 10^{-24} a_{H^+}^{-1}$	No data	Thinnappan et al. (2008) (105)
Merrillite	$Ca_{9.5}Mg(PO_4)_7$	1070	3.1	2-5	log R = -0.92 × pH – 4.56	No data	Adcock et al. (2013) (83)
Struvite	$MgNH_4PO_4 \cdot 6H_2O$	245.4	1.7	7-11	Constant (-8.85)	44.8	Roncal-Herrero & Oelkers (2011) (32); Babić-Ivančić et al. (2002)(106)
Whitlockite	$Ca_9Mg(HPO_4)(PO_4)_6$	1051	3.1	2-5	log R = -0.95 × pH -4.50	No data	Adcock et al. (2013) (83)

[a]Density from mindat.org; [b]Kinetic experiment at 25 °C except vivianite (18.5 °C).

Table S6. Calculated abundances of elements in Enceladus's ocean based on model assumptions.

Element	CI chondrites[a]	Molecular weight	c (max from rock)[b]	c(pH = 8.5)[c]		c(pH = 11)[c]	
	ppm (ug/g)	g/mole	mole/kg H_2O	High Carbonate[d]	Low Carbonate[e]	High Carbonate[f]	Low Carbonate[g]
C	35180	12.011	1.03E+01	1.00E-01	1.02E-02	1.00E-01	1.00E-02
N	2940	14.007	7.35E-01	1.00E-03	1.30E-04	3.90E-07	8.00E-08
F	60.6	18.998	1.12E-02	2.53E-02	8.00E-03	2.10E-02	7.84E-03
Na	5010	22.99	7.63E-01	3.25E-01	6.52E-02	4.04E-01	7.56E-02
Mg	95870	24.305	1.38E+01	3.51E-04	1.14E-03	3.51E-07	9.95E-08
Si	106500	28.085	1.33E+01	2.33E-05	2.33E-05	1.79E-04	1.58E-04
P	920	30.974	1.04E-01	8.80E-04	2.61E-05	2.08E-06	7.49E-08
Cl	704	35.45	6.95E-02	2.00E-01	5.00E-02	2.00E-01	5.00E-02
K	530	39.098	4.74E-02	3.25E-03	6.50E-04	4.04E-03	7.50E-04
Ca	9070	40.078	7.92E-01	9.50E-07	3.10E-06	6.63E-06	8.71E-06
Fe	182800	55.845	1.15E+01	1.03E-05	1.18E-05	1.32E-07	2.54E-08

[a]Average abundances of elements in CI chondrites (19); [b]concentration of elements assuming total dissolution from Enceladus's core (7×10^{19} kg rock) into the global ocean (2×10^{19} kg water); [c]concentration of elements (mole/kg H_2O) in our nominal model runs (N/CO_2 molar ratio = 1.5) at 0 °C and with F as an example (see **Fig. S2** for more results in graphical form); [d]equilibrium minerals present (**Fig. S3A**): magnesite, dolomite, siderite, fluorite, quartz, F-apatite, struvite (close to saturation), chalcedony (close to saturation); [e]equilibrium minerals present (**Fig. S3C**): magnesite, dolomite, siderite, fluorite, quartz, F-apatite, chalcedony (close to saturation); [f]equilibrium minerals present (**Fig. S3A**): talc, calcite, greenalite, fluorite, quartz, F-apatite, aragonite (close to saturation), chalcedony (close to saturation), dolomite (close to saturation); [g]equilibrium minerals present (**Fig. S3C**): talc, calcite, greenalite, fluorite, quartz, F-apatite, aragonite (close to saturation), chalcedony (close to saturation).

Table S7. pH of the point of zero charge (pH_{pzc}) of minerals. In Enceladus ocean water (estimated pH between 8.5 and 11), all of the listed minerals would have net negatively charged surfaces.

Mineral name	Formula	pH_{pzc}	Data source
Ferrihydrite	$Fe_{10}O_{14}(OH)_2$	8	Hiemstra (2013) (107)
Green rust	$Fe_6(OH)_{12}(CO_3,SO_4)$	8.3	Guilbaud et al. (2013) (47)
Calcite	$CaCO_3$	8	Santos et al. (2015) (108)
Siderite	$FeCO_3$	5.3	Charlet et al. (1990) (109)
Magnesite	$MgCO_3$	6.7	Chen & Tao (2005) (110)
Dolomite	$CaMg(CO_3)_2$	6.3	Chen & Tao (2005) (110)
Quartz	SiO_2	3	Sverjensky & Sahai (1996) (111)
Amorphous silica	$SiO_2 * nH_2O$	2.8	Sverjensky (2006) (112)
Tremolite	$Ca_2Mg_5Si_8O_{22}(OH)_2$	6.7	Sverjensky & Sahai (1996) (111)
Talc	$Mg_3Si_4O_{10}(OH)_2$	6.7	Sverjensky & Sahai (1996) (111)
Lizardite	$Mg_3Si_2O_5(OH)_4$	4.3	Alvarez-Silva et al. (2010) (113)
Vivianite	$Fe_3(PO_4)_2 * 8H_2O$	5.3	Thinnappan et al. (2008) (105)
OH-apatite	$Ca_5(PO_4)_3(OH)$	8.5	Bell et al. (1973) (114)
F-apatite	$Ca_5(PO_4)_3F$	6.7	Bell et al. (1973) (114)
Fluorite	CaF_2	8.2	Jiang et al. (2018) (115)

SI References

1. F. Postberg, *et al.*, Sodium salts in E-ring ice grains from an ocean below the surface of Enceladus. *Nature* (2009) https:/doi.org/10.1038/nature08046.
2. J. S. Kargel, *et al.*, Europa's Crust and Ocean: Origin, Composition, and the Prospects for Life. *Icarus* (2000) https:/doi.org/10.1006/icar.2000.6471.
3. F. Dhooghe, *et al.*, Chlorine-bearing species and the 37Cl/35Cl isotope ratio in the coma of comet 67P/Churyumov–Gerasimenko. *Mon. Not. R. Astron. Soc.* **508**, 1020–1032 (2021).
4. J. H. Waite, *et al.*, Cassini finds molecular hydrogen in the Enceladus plume: Evidence for hydrothermal processes. *Science (80-.).* (2017) https:/doi.org/10.1126/science.aai8703.
5. H.-W. Hsu, *et al.*, Ongoing hydrothermal activities within Enceladus. *Nature* **519**, 207–210 (2015).
6. A. J. Brearley, "The action of water" in *Meteorites and the Early Solar System II*, (2006).
7. A. N. Krot, *et al.*, "Timescales and settings for alteration of chondritic meteorites" (Lawrence Livermore National Lab.(LLNL), Livermore, CA (United States), 2005).
8. C. R. Glein, J. H. Waite, The Carbonate Geochemistry of Enceladus' Ocean. *Geophys. Res. Lett.* (2020) https:/doi.org/10.1029/2019GL085885.
9. P. L. Clay, *et al.*, Halogens in chondritic meteorites and terrestrial accretion. *Nature* (2017) https:/doi.org/10.1038/nature24625.
10. F. Pirajno, "Halogens in Hydrothermal Fluids and Their Role in the Formation and Evolution of Hydrothermal Mineral Systems" in *The Role of Halogens in Terrestrial and Extraterrestrial Geochemical Processes: Surface, Crust, and Mantle*, D. E. Harlov, L. Aranovich, Eds. (Springer International Publishing, 2018), pp. 759–804.
11. R. Siever, The silica cycle in the Precambrian. *Geochim. Cosmochim. Acta* **56**, 3265–3272 (1992).
12. R. Siever, Burial history and diagenetic reaction kinetics. *Am. Assoc. Pet. Geol. Bull.* (1983) https:/doi.org/10.1306/03B5B67D-16D1-11D7-8645000102C1865D.
13. L. A. Williams, G. A. Parks, D. A. Crerar, Silica diagenesis: I. Solubility controls. *J. Sediment. Petrol.* (1985) https:/doi.org/10.1306/212f86ac-2b24-11d7-8648000102c1865d.
14. R. O. Fournier, The Behavior of Silica in Hydrothermal Solutions. *Geol. Geochemistry Ep. Syst.* **2**, 0 (1985).
15. N. J. Tosca, A. H. Knoll, Juvenile chemical sediments and the long term persistence of water at the surface of Mars. *Earth Planet. Sci. Lett.* (2009) https:/doi.org/10.1016/j.epsl.2009.07.004.
16. M. Ćuk, L. Dones, D. Nesvorný, Dynamical Evidence for a Late Formation of Saturn'S Moons. *Astrophys. J.* **820**, 97 (2016).
17. M. Neveu, A. R. Rhoden, Evolution of Saturn's mid-sized moons. *Nat. Astron.* (2019) https:/doi.org/10.1038/s41550-019-0726-y.
18. T. J. Wolery, *EQ3/6: A software package for geochemical modeling of aqueous systems: package overview and installation guide (version 7.0)* (Lawrence Livermore National Laboratory Livermore, CA, 1992).
19. K. Lodders, Solar System Abundances and Condensation Temperatures of the Elements. *Astrophys. J.* (2003) https:/doi.org/10.1086/375492.
20. K. Altwegg, *et al.*, Prebiotic chemicals--amino acid and phosphorus--in the coma of comet 67P/Churyumov-Gerasimenko. *Sci. Adv.* **2**, e1600285–e1600285 (2016).
21. Y. Sekine, *et al.*, High-temperature water-rock interactions and hydrothermal environments in the chondrite-like core of Enceladus. *Nat. Commun.* (2015) https:/doi.org/10.1038/ncomms9604.
22. J. W. Johnson, E. H. Oelkers, H. C. Helgeson, SUPCRT92: A software package for calculating the standard molal thermodynamic properties of minerals, gases, aqueous species, and reactions from 1 to 5000 bar and 0 to 1000??C. *Comput. Geosci.* **18**, 899–947 (1992).
23. R. G. Berman, Internally-Consistent Thermodynamic Data for Minerals in the System Na2o-K2o-Cao-Mgo-Feo-Fe2o3-Al2o3-Sio2-Tio2-H2o-Co2. *J. Petrol.* **29**, 445–522 (1988).

24. C. Zhu, D. A. Sverjensky, Partitioning of F-Cl-OH between minerals and hydrothermal fluids. *Geochim. Cosmochim. Acta* (1991) https:/doi.org/10.1016/0016-7037(91)90028-4.
25. R. H. Worden, “Halogen Elements in Sedimentary Systems and Their Evolution During Diagenesis” in *The Role of Halogens in Terrestrial and Extraterrestrial Geochemical Processes: Surface, Crust, and Mantle*, D. E. Harlov, L. Aranovich, Eds. (Springer International Publishing, 2018), pp. 185–260.
26. R. A. Gulbrandsen, Physical and chemical factors in the formation of marine apatite. *Econ. Geol.* (1969) https:/doi.org/10.2113/gsecongeo.64.4.365.
27. J. D. Toner, D. C. Catling, A carbonate-rich lake solution to the phosphate problem of the origin of life. *Proc. Natl. Acad. Sci. U. S. A.* **117**, 883–888 (2020).
28. K. Fukushi, *et al.*, In Situ Formation of Monohydrocalcite in Alkaline Saline Lakes of the Valley of Gobi Lakes: Prediction for Mg, Ca, and Total Dissolved Carbonate Concentrations in Enceladus’ Ocean and Alkaline-Carbonate Ocean Worlds. *Miner.* **10** (2020).
29. N. Zeyen, *et al.*, Integrative analysis of the mineralogical and chemical composition of modern microbialites from ten Mexican lakes: What do we learn about their formation? *Geochim. Cosmochim. Acta* **305**, 148–184 (2021).
30. M. A. Pasek, Rethinking early Earth phosphorus geochemistry. *Proc. Natl. Acad. Sci. U. S. A.* (2008) https:/doi.org/10.1073/pnas.0708205105.
31. R. M. Garrels, C. L. Christ, *Solutions, minerals, and equilibria* (Harper & Row, 1965).
32. T. Roncal-Herrero, E. H. Oelkers, Experimental determination of struvite dissolution and precipitation rates as a function of pH. *Appl. Geochemistry* (2011) https:/doi.org/10.1016/j.apgeochem.2011.03.002.
33. J. O. Nriagu, P. B. Moore, *Phosphate Minerals*, J. O. Nriagu, P. B. Moore, Eds., 1st Ed. (Springer -Verlag Berlin Heidelberg New York Tokyo, 1984) https:/doi.org/10.1007/978-3-642-61736-2.
34. N. Khawaja, *et al.*, Low-mass nitrogen-, oxygen-bearing, and aromatic compounds in Enceladean ice grains. *Mon. Not. R. Astron. Soc.* (2019) https:/doi.org/10.1093/mnras/stz2280.
35. C. F. Conrad, *et al.*, Modeling the kinetics of silica nanocolloid formation and precipitation in geologically relevant aqueous solutions. *Geochim. Cosmochim. Acta* **71**, 531–542 (2007).
36. N. M. Fernandez, X. Zhang, J. L. Druhan, Silicon isotopic re-equilibration during amorphous silica precipitation and implications for isotopic signatures in geochemical proxies. *Geochim. Cosmochim. Acta* **262**, 104–127 (2019).
37. J. Compton, *et al.*, Variations in the Global Phosphorus Cycle. *Mar. Authigenes. From Glob. to Microb.*, 21–33 (2000).
38. A. Paytan, K. McLaughlin, The oceanic phosphorus cycle. *Chem. Rev.* **107**, 563–576 (2007).
39. K. C. Ruttenberg, “The Global Phosphorus Cycle” in *Treatise on Geochemistry: Second Edition*, (2013) https:/doi.org/10.1016/B978-0-08-095975-7.00813-5.
40. M. L. Delaney, Phosphorus accumulation in marine sediments and the oceanic phosphorus cycle. *Global Biogeochem. Cycles* (1998) https:/doi.org/10.1029/98GB02263.
41. C. G. Wheat, R. A. Feely, M. J. Mottl, Phosphate removal by oceanic hydrothermal processes: An update of the phosphorus budget in the oceans. *Geochim. Cosmochim. Acta* **60**, 3593–3608 (1996).
42. K. Barthélémy, S. Naille, C. Despas, C. Ruby, M. Mallet, Carbonated ferric green rust as a new material for efficient phosphate removal. *J. Colloid Interface Sci.* **384**, 121–127 (2012).
43. I. Halevy, M. Alesker, E. M. Schuster, R. Popovitz-Biro, Y. Feldman, A key role for green rust in the Precambrian oceans and the genesis of iron formations. *Nat. Geosci.* **10**, 135 (2017).
44. N. J. Tosca, C. Z. Jiang, B. Rasmussen, J. Muhling, Products of the iron cycle on the early Earth. *Free Radic. Biol. Med.* (2019) https:/doi.org/10.1016/j.freeradbiomed.2019.05.005.

45. J. E. Johnson, J. R. Muhling, J. Cosmidis, B. Rasmussen, A. S. Templeton, Low-Fe(III) Greenalite Was a Primary Mineral From Neoarchean Oceans. *Geophys. Res. Lett.* **45**, 3182–3192 (2018).
46. D. J. Hemingway, T. Mittal, Enceladus's ice shell structure as a window on internal heat production. *Icarus* **332**, 111–131 (2019).
47. R. Guilbaud, M. L. White, S. W. Poulton, Surface charge and growth of sulphate and carbonate green rust in aqueous media. *Geochim. Cosmochim. Acta* **108**, 141–153 (2013).
48. C. Mangwandi, A. B. Albadarin, Y. Glocheux, G. M. Walker, Removal of ortho-phosphate from aqueous solution by adsorption onto dolomite. *J. Environ. Chem. Eng.* (2014) https:/doi.org/10.1016/j.jece.2014.04.010.
49. R. D. Van Der Weijden, J. Meima, R. N. J. Comans, Sorption and sorption reversibility of cadmium on calcite in the presence of phosphate and sulfate. *Mar. Chem.* (1997) https:/doi.org/10.1016/S0304-4203(97)00018-2.
50. C. E. Cowan, J. M. Zachara, C. T. Resch, Solution ion effects on the surface exchange of selenite on calcite. *Geochim. Cosmochim. Acta* (1990) https:/doi.org/10.1016/0016-7037(90)90047-O.
51. B. Wang, *et al.*, Novel talc encapsulated lanthanum alginate hydrogel for efficient phosphate adsorption and fixation. *Chemosphere* (2020) https:/doi.org/10.1016/j.chemosphere.2020.127124.
52. F. Millero, F. Huang, X. Zhu, X. Liu, J. Z. Zhang, Adsorption and desorption of phosphate on calcite and aragonite in seawater. *Aquat. Geochemistry* **7**, 33–56 (2001).
53. D. Kiani, M. Silva, Y. Sheng, J. Baltrusaitis, Experimental Insights into the Genesis and Growth of Struvite Particles on Low-Solubility Dolomite Mineral Surfaces. *J. Phys. Chem. C* (2019) https:/doi.org/10.1021/acs.jpcc.9b05292.
54. K. Karageorgiou, M. Paschalis, G. N. Anastassakis, Removal of phosphate species from solution by adsorption onto calcite used as natural adsorbent. *J. Hazard. Mater.* (2007) https:/doi.org/10.1016/j.jhazmat.2006.02.038.
55. L. Iess, *et al.*, The gravity field and interior structure of Enceladus. *Science (80-.).* (2014) https:/doi.org/10.1126/science.1250551.
56. P. C. Thomas, *et al.*, Enceladus's measured physical libration requires a global subsurface ocean. *Icarus* (2016) https:/doi.org/10.1016/j.icarus.2015.08.037.
57. G. Choblet, *et al.*, Powering prolonged hydrothermal activity inside Enceladus. *Nat. Astron.* (2017) https:/doi.org/10.1038/s41550-017-0289-8.
58. G. Tobie, O. Čadek, C. Sotin, Solid tidal friction above a liquid water reservoir as the origin of the south pole hotspot on Enceladus. *Icarus* (2008) https:/doi.org/10.1016/j.icarus.2008.03.008.
59. A. C. Campbell, *et al.*, Chemistry of hot springs on the Mid-Atlantic Ridge. *Nature* (1988) https:/doi.org/10.1038/335514a0.
60. C. G. Wheat, A. T. Fisher, J. McManus, S. M. Hulme, B. N. Orcutt, Cool seafloor hydrothermal springs reveal global geochemical fluxes. *Earth Planet. Sci. Lett.* (2017) https:/doi.org/10.1016/j.epsl.2017.07.049.
61. R. P. Lowell, M. DuBose, Hydrothermal systems on Europa. *Geophys. Res. Lett.* **32** (2005).
62. E. L. Steel, A. Davila, C. P. McKay, Abiotic and Biotic Formation of Amino Acids in the Enceladus Ocean. *Astrobiology* **17**, 862–875 (2017).
63. C. R. Glein, F. Postberg, S. D. Vance, "The Geochemistry of Enceladus: Composition and Controls" in *Enceladus and the Icy Moons of Saturn*, (2018) https:/doi.org/10.2458/azu_uapress_9780816537075-ch003.
64. M. Y. Zolotov, Aqueous fluid composition in CI chondritic materials: Chemical equilibrium assessments in closed systems. *Icarus* (2012) https:/doi.org/10.1016/j.icarus.2012.05.036.
65. M. Y. Zolotov, An oceanic composition on early and today's Enceladus. *Geophys. Res. Lett.* (2007) https:/doi.org/10.1029/2007GL031234.
66. T. M. Gregory, E. C. Moreno, J. M. Patel, W. E. Brown, Solubility of β-Ca(3)(PO(4))(2) in the System Ca(OH)(2)-H(3)PO(4)-H(2)O at 5, 15, 25, and 37 °C. *J. Res. Natl. Bur. Stand. Sect. A, Phys. Chem.* **78A**, 667–674 (1974).

67. M. Y. Zolotov, M. V Mironenko, E. L. Shock, Thermodynamic constraints on fayalite formation on parent bodies of chondrites. *Meteorit. Planet. Sci.* **41**, 1775–1796 (2006).
68. D. E. LaRowe, H. C. Helgeson, Biomolecules in hydrothermal systems: Calculation of the standard molal thermodynamic properties of nucleic-acid bases, nucleosides, and nucleotides at elevated temperatures and pressures. *Geochim. Cosmochim. Acta* **70**, 4680–4724 (2006).
69. J. M. Dick, CHNOSZ: Thermodynamic Calculations and Diagrams for Geochemistry . *Front. Earth Sci.* **7** (2019).
70. E. L. Shock, D. C. Sassani, M. Willis, D. a Sverjensky, Inorganic species in geologic fluids: Correlations among standard molal thermodynamic properties of aqueous ions and hydroxide complexes. *Geochim. Cosmochim. Acta* **61**, 907–950 (1997).
71. A. C. Lasaga, *Kinetic theory in the earth sciences* (Princeton University Press, 1998) https:/doi.org/10.5860/choice.36-4499.
72. N. C. M. Marty, *et al.*, A database of dissolution and precipitation rates for clay-rocks minerals. *Appl. Geochemistry* **55**, 108–118 (2015).
73. J. W. Zhang, G. H. Nancollas, Mechanisms of growth and dissolution of sparingly soluble salts. *Rev. Mineral. Geochemistry* **23**, 365–396 (1990).
74. S. M. Hamza, S. K. Hamdona, Kinetics of dissolution of calcium fluoride crystals in sodium chloride solutions: influence of additives. *J. Phys. Chem.* **95**, 3149–3152 (1991).
75. J. L. Palandri, Y. K. Kharaka, "A compilation of rate parameters of water-mineral interaction kinetics for application to geochemical modeling" (Geological Survey Menlo Park CA, 2004).
76. G. D. Saldi, S. J. Köhler, N. Marty, E. H. Oelkers, Dissolution rates of talc as a function of solution composition, pH and temperature. *Geochim. Cosmochim. Acta* **71**, 3446–3457 (2007).
77. M. Rozalen, *et al.*, Dissolution study of tremolite and anthophyllite: pH effect on the reaction kinetics. *Appl. Geochemistry* **49**, 46–56 (2014).
78. M. D. Schulte, E. L. Shock, R. H. Wood, The temperature dependence of the standard-state thermodynamic properties of aqueous nonelectrolytes. *Geochim. Cosmochim. Acta* (2001) https:/doi.org/10.1016/S0016-7037(01)00717-7.
79. D. A. Sverjensky, B. Harrison, D. Azzolini, Water in the deep Earth: The dielectric constant and the solubilities of quartz and corundum to 60 kb and 1200 °C. *Geochim. Cosmochim. Acta* **129**, 125–145 (2014).
80. C. R. Glein, J. A. Baross, J. Hunter Waite, The pH of Enceladus' ocean. *Geochim. Cosmochim. Acta* (2015) https:/doi.org/10.1016/j.gca.2015.04.017.
81. J. H. Waite Jr, *et al.*, Liquid water on Enceladus from observations of ammonia and 40Ar in the plume. *Nature* **460**, 487–490 (2009).
82. H. T. Smith, *et al.*, Enceladus: A potential source of ammonia products and molecular nitrogen for Saturn's magnetosphere. *J. Geophys. Res. Sp. Phys.* **113** (2008).
83. C. T. Adcock, E. M. Hausrath, P. M. Forster, Readily available phosphate from minerals in early aqueous environments on Mars. *Nat. Geosci.* (2013) https:/doi.org/10.1038/ngeo1923.
84. A. La Iglesia, Estimating the thermodynamic properties of phosphate minerals at high and low temperature from the sum of constituent units. *Estud. Geol.* (2009) https:/doi.org/10.3989/egeol.39849.060.
85. H. Mcdowell, W. E. Brown, J. R. Sutter, Solubility Study of Calcium Hydrogen Phosphate. Ion-Parr Formation. *Inorg. Chem.* (1971) https:/doi.org/10.1021/ic50102a020.
86. A. Al-Borno, M. B. Tomson, The temperature dependence of the solubility product constant of vivianite. *Geochim. Cosmochim. Acta* (1994) https:/doi.org/10.1016/0016-7037(94)90236-4.
87. G. J. Racz, R. J. Soper, SOLUBILITY OF DIMAGNESIUM PHOSPHATE TRIHYDRATE AND TRIMAGNESIUM PHOSPHATE. *Can. J. Soil Sci.* (1968) https:/doi.org/10.4141/cjss68-036.
88. A. W. Taylor, A. W. Frazier, E. L. Gurney, Solubility products of magnesium ammonium and magnesium potassium phosphates. *Trans. Faraday Soc.* (1963) https:/doi.org/10.1039/tf9635901580.

89. B. B. Luff, R. B. Reed, Thermodynamic Properties of Magnesium Potassium Orthophosphate Hexahydrate. *J. Chem. Eng. Data* (1980) https:/doi.org/10.1021/je60087a028.
90. K. Xu, *et al.*, The precipitation of magnesium potassium phosphate hexahydrate for P and K recovery from synthetic urine. *Water Res.* (2015) https:/doi.org/10.1016/j.watres.2015.05.026.
91. P. R. Patel, T. M. Gregory, W. E. Brown, Solubility of CaHPO4· 2H2O in the Quaternary System Ca (OH) 2− H3PO4− NaCl− H2O at 25° C. *J. Res. Natl. Bur. Stand. Sect. A, Phys. Chem.* **78**, 675 (1974).
92. M. S. Tung, N. Eidelman, B. Sieck, W. E. Brown, Octacalcium Phosphate Solubility Product from 4 to 37-Degree-C. *J. Res. Natl. Bur. Stand. (1934).* (1988) https:/doi.org/10.6028/jres.093.153.
93. M. I. H. Bhuiyan, D. S. Mavinic, R. D. Beckie, A solubility and thermodynamic study of struvite. *Environ. Technol.* (2007) https:/doi.org/10.1080/09593332808618857.
94. J. O. Nriagu, Solubility equilibrium constant of strengite. *Am. J. Sci.* (1972) https:/doi.org/10.2475/ajs.272.5.476.
95. E. P. Egan, Z. T. Wakefield, B. B. Luff, Low temperature heat capacity, entropy and heat of formation of crystalline and colloidal ferric phosphate dihydrate. *J. Phys. Chem.* (1961) https:/doi.org/10.1021/j100825a041.
96. P. Vieillard, *Géochimie des phosphates. Étude thermodynamique. Application à la genèse et à l'altération des apatites* (Persée-Portail des revues scientifiques en SHS, 1978).
97. A. E. RUBIN, Mineralogy of meteorite groups: An update. *Meteorit. Planet. Sci.* (1997) https:/doi.org/10.1111/j.1945-5100.1997.tb01558.x.
98. A. E. Rubin, Mineralogy of meteorite groups. *Meteorit. Planet. Sci.* (1997) https:/doi.org/10.1111/j.1945-5100.1997.tb01262.x.
99. A. E. Rubin, J. M. Trigo-Rodríguez, H. Huber, J. T. Wasson, Progressive aqueous alteration of CM carbonaceous chondrites. *Geochim. Cosmochim. Acta* **71**, 2361–2382 (2007).
100. C. R. Walton, *et al.*, Phosphorus mineral evolution and prebiotic chemistry: From minerals to microbes. *Earth-Science Rev.* **221**, 103806 (2021).
101. T. Feng, M. Gull, A. Omran, H. Abbott-Lyon, M. A. Pasek, Evolution of Ephemeral Phosphate Minerals on Planetary Environments. *ACS Earth Sp. Chem.* **5**, 1647–1656 (2021).
102. C. Chaïrat, J. Schott, E. H. Oelkers, J. E. Lartigue, N. Harouiya, Kinetics and mechanism of natural fluorapatite dissolution at 25 °C and pH from 3 to 12. *Geochim. Cosmochim. Acta* (2007) https:/doi.org/10.1016/j.gca.2007.08.031.
103. N. Harouiya, C. Chaïrat, S. J. Köhler, R. Gout, E. H. Oelkers, The dissolution kinetics and apparent solubility of natural apatite in closed reactors at temperatures from 5 to 50 °C and pH from 1 to 6. *Chem. Geol.* (2007) https:/doi.org/10.1016/j.chemgeo.2007.07.011.
104. J. Oliva, J. Cama, J. L. Cortina, C. Ayora, J. De Pablo, Biogenic hydroxyapatite (Apatite II™) dissolution kinetics and metal removal from acid mine drainage. *J. Hazard. Mater.* (2012) https:/doi.org/10.1016/j.jhazmat.2012.01.027.
105. V. Thinnappan, *et al.*, A combined experimental study of vivianite and As (V) reactivity in the pH range 2–11. *Appl. Geochemistry* **23**, 3187–3204 (2008).
106. V. Babić-Ivančić, J. Kontrec, D. Kralj, L. Brečević, Precipitation diagrams of struvite and dissolution kinetics of different struvite morphologies. *Croat. Chem. Acta* (2002).
107. T. Hiemstra, Surface and mineral structure of ferrihydrite. *Geochim. Cosmochim. Acta* **105**, 316–325 (2013).
108. E. P. Santos, A. J. B. Dutra, J. F. Oliveira, The effect of jojoba oil on the surface properties of calcite and apatite aiming at their selective flotation. *Int. J. Miner. Process.* (2015) https:/doi.org/10.1016/j.minpro.2015.08.002.
109. L. Charlet, P. Wersin, W. Stumm, Surface charge of MnCO3and FeCO3. *Geochim. Cosmochim. Acta* (1990) https:/doi.org/10.1016/0016-7037(90)90059-T.
110. G. L. Chen, D. Tao, Reverse Flotation of Magnesite by Dodecyl Phosphate from Dolomite in the Presence of Sodium Silicate. *Sep. Sci. Technol.* (2005) https:/doi.org/10.1081/ss-120027564.

111. D. A. Sverjensky, N. Sahai, Theoretical prediction of single-site surface-protonation equilibrium constants for oxides and silicates in water. *Geochim. Cosmochim. Acta* (1996) https:/doi.org/10.1016/0016-7037(96)00207-4.
112. D. A. Sverjensky, Prediction of the speciation of alkaline earths adsorbed on mineral surfaces in salt solutions. *Geochim. Cosmochim. Acta* (2006) https:/doi.org/10.1016/j.gca.2006.01.006.
113. M. Alvarez-Silva, A. Uribe-Salas, M. Mirnezami, J. A. Finch, The point of zero charge of phyllosilicate minerals using the Mular-Roberts titration technique. *Miner. Eng.* (2010) https:/doi.org/10.1016/j.mineng.2009.11.013.
114. L. C. Bell, A. M. Posner, J. P. Quirk, The point of zero charge of hydroxyapatite and fluorapatite in aqueous solutions. *J. Colloid Interface Sci.* (1973) https:/doi.org/10.1016/0021-9797(73)90288-9.
115. W. Jiang, *et al.*, Selective adsorption of benzhydroxamic acid on fluorite rendering selective separation of fluorite/calcite. *Appl. Surf. Sci.* (2018) https:/doi.org/10.1016/j.apsusc.2017.11.093.